



LUND UNIVERSITY

Interacting Giants and Compact Stars

Bobrick, Alexey

2021

[Link to publication](#)

Citation for published version (APA):

Bobrick, A. (2021). *Interacting Giants and Compact Stars*. [Doctoral Thesis (compilation)]. Lund University (Media-Tryck).

Total number of authors:

1

General rights

Unless other specific re-use rights are stated the following general rights apply:

Copyright and moral rights for the publications made accessible in the public portal are retained by the authors and/or other copyright owners and it is a condition of accessing publications that users recognise and abide by the legal requirements associated with these rights.

- Users may download and print one copy of any publication from the public portal for the purpose of private study or research.
- You may not further distribute the material or use it for any profit-making activity or commercial gain
- You may freely distribute the URL identifying the publication in the public portal

Read more about Creative commons licenses: <https://creativecommons.org/licenses/>

Take down policy

If you believe that this document breaches copyright please contact us providing details, and we will remove access to the work immediately and investigate your claim.

LUND UNIVERSITY

PO Box 117
221 00 Lund
+46 46-222 00 00

Interacting Giants and Compact Stars

ALEXEY BOBRICK

DEPT. OF ASTRONOMY AND THEORETICAL PHYSICS | LUND UNIVERSITY 2021



Interacting Giants and Compact Stars

Interacting Giants and Compact Stars

Alexey Bobrick



LUND
UNIVERSITY

Thesis for the degree of Doctor of Philosophy

Thesis advisor: Prof. Melvyn B. Davies

Co-advisor: Prof. Lennart Lindegren

Faculty opponent: Prof. Thomas Tauris

To be presented, with the permission of the Faculty of Science of Lund University, for public criticism in the Lundmark lecture hall (Lundmarksalen) at the Department of Astronomy and Theoretical Physics and online via video broadcasting facilitated by Lund University Conference Services on Thursday 17th June 2021 at 13:00.

Organization LUND UNIVERSITY Department of Astronomy and Theoretical Physics Box 43, SE-22100 Lund, Sweden		Document name DOCTORAL DISSERTATION	
		Date of issue 2021-06-17	
Author(s) Alexey Bobrick (Aliaksei Bobryk)		Sponsoring organization	
Title and subtitle Interacting Giants and Compact Stars			
Abstract <p>This thesis is based on four papers dealing with various aspects of interactions in binary stars. Interactions between stars occur at nearly all stages of their evolution and can take many forms. For example, stars may lose material to a binary companion, merge, interact with groups of other stars in star clusters and explode in binary systems, among other interactions.</p> <p>The first paper in this thesis, Bobrick et al. (2017) (Paper I), models how white dwarfs interact with neutron stars as they spiral into contact due to gravitational wave emission. Through the use of hydrodynamic simulations with the Oil-on-Water code, we investigated the process of mass transfer in such binaries. We found that early phases of interactions in these systems lead to significant loss of angular momentum, driving systems to merge more often than previously expected. The third paper in the thesis, Bobrick et al. (2021a) (Paper III), describes the subsequent evolution of the white dwarf-neutron star binaries containing a massive white dwarf after they merge. In this case, the white dwarf gets shredded into a disc, reaching high temperatures leading to nuclear reactions. These nuclear reactions in the disc produce nickel-56 that gets ejected with the rest of the material from the vicinity of the neutron star. As the ejected material expands, the radioactive nickel-56 heats the material, causing it to glow and become observable as a supernova-like transient event. We used hydrodynamic simulations based on the Water code and a nuclear processing code Torch to study nucleosynthesis in the disc, and a supernova spectral synthesis code SuperNu to model how these events may be observed.</p> <p>Unlike papers I and III, which dealt with compact objects, papers II and IV focussed on interactions involving giant stars. In the second paper, Vos et al. (2020) (Paper II), we modelled how mass transfer between red giants and main-sequence stars can give rise to subdwarf B stars. These subdwarf B stars are remnant cores of the red giants that ignited helium while losing mass. By performing a population study based on detailed stellar structure code MESA, we found that the orbits of such subdwarf B binaries bear imprints of the chemical history of our Galaxy. The fact that the Milky Way had changed its metal content over time allowed us to explain the orbital periods of the known subdwarf B binaries. In our fourth study, Bobrick et al. (2021b) (Paper IV), we investigated the formation history of Betelgeuse, which is a red supergiant visible to the naked eye. It has been recently realised that Betelgeuse is likely an outcome of a merger between two stars that were ejected from their birth environment. To test this scenario, we used the FewBody code together with a Monte Carlo-based model of dynamical interactions in the Milky Way star clusters and synthesised a population of stars which may lead to the formation of Betelgeuse. We have confirmed that a stellar merger is indeed a likely mechanism behind the formation of Betelgeuse.</p>			
Key words (stars) Binaries; General; (stars); neutron; (stars); subdwarfs; (stars); supergiants; hydrodynamics; nuclear reactions, nucleosynthesis, abundances			
Classification system and/or index terms (if any)			
Supplementary bibliographical information		Language English	
ISSN and key title		ISBN 978-91-7895-901-3 (print) 978-91-7895-902-0 (pdf)	
Recipient's notes		Number of pages 164	
		Price	
		Security classification	

I, the undersigned, being the copyright owner of the abstract of the above-mentioned dissertation, hereby grant to all reference sources permission to publish and disseminate the abstract of the above-mentioned dissertation.

Signature



Date 2021-05-04

Interacting Giants and Compact Stars

Alexey Bobrick



LUND
UNIVERSITY

Faculty Opponent

Prof. Thomas Tauris
Department of Physics and Astronomy, Aarhus University,
Aarhus Institute of Advanced Studies (AIAS), Aarhus University
Aarhus, Denmark

Evaluation Committee

Dr Josefin Larsson
Department of Physics, KTH Royal Institute of Technology
The Oskar Klein Centre
Stockholm, Sweden

Prof. Stephen Justham
School of Astronomy and Space Science
University of the Chinese Academy of Sciences,
National Astronomical Observatories, Chinese Academy of Sciences
Beijing, China
Anton Pannekoek Institute for Astronomy, University of Amsterdam
GRAPPA, University of Amsterdam
Amsterdam, The Netherlands

Prof. Paul Callanan
Department of Physics, University College Cork
Cork, Ireland

Front cover: Density snapshot from a 3D simulation from Bobrick et al. (2017) (Paper I) of a mass-transferring white dwarf-neutron star binary with a low-mass helium white dwarf. The figure shows the white dwarf donor, the stream of the transferred material, the disc formed around the neutron star and a cloud of material forming around the binary.

© Alexey Bobrick 2021

Faculty of Science, Department of Astronomy and Theoretical Physics

ISBN: 978-91-7895-901-3 (print)

ISBN: 978-91-7895-902-0 (pdf)

Printed in Sweden by Media-Tryck, Lund University, Lund 2021



To the memory of my grandfather

Contents

List of publications	ii
Work not included in the thesis	iii
Popular summary	v
Populärvetenskaplig sammanfattning	vii
Acknowledgements	ix
Interacting Giants and Compact Stars	1
1 Physics of stellar interactions	5
2 Modelling stellar interactions	28
3 Comparing models against observations	40
Scientific publications	63
Paper summaries and author contributions	63
Paper I: Mass transfer in white dwarf-neutron star binaries	67
Paper II: Observed binary populations reflect the Galactic history. Explaining the orbital period-mass ratio relation in wide hot subdwarf binaries.	89
Paper III: Transients from ONe White-Dwarf - Neutron-Star/Black Hole Mergers	111
Paper IV: Production of Rapidly-Spinning Runaway Red Supergiants	133

List of publications

This thesis is based on the following peer-reviewed publications:

- I **Mass transfer in white dwarf-neutron star binaries.**
Bobrick, A.; Davies, M.B.; Church, R.P. (2017)
MNRAS, Volume 467, Issue 3 (23 pp.)
- II **Observed binary populations reflect the Galactic history. Explaining the orbital period-mass ratio relation in wide hot subdwarf binaries.**
Vos, J.; Bobrick, A.; M. Vučković (2020)
Astronomy and Astrophysics, Volume 641, A163 (19 pp.)
- III **Transients from ONe White-Dwarf - Neutron-Star/Black Hole Mergers**
Bobrick, A.; Zenati, Y.; Perets, H.; Church, R.P.; Davies, M.B. (2021)
Submitted to MNRAS (20 pp.)
- IV **Production of Rapidly-Spinning Runaway Red Supergiants**
Bobrick, A.; Raddi, R.; Chatzopoulos, E.; Church, R.P.; Davies, M.B.; Frank, J. (2021)
To be submitted to MNRAS (12 pp.)

Paper I is reproduced with permission from the MNRAS journal (Oxford University Press). Paper II is reproduced with permission from Astronomy & Astrophysics © ESO. Papers III and IV are the submitted and draft versions of the papers, respectively, for the MNRAS journal.

Work not included in the thesis

Peer-reviewed publications not included in this thesis:

- I **Formation constraints indicate a black-hole accretor in 47 Tuc X9.**
Church, R.P.; Strader, J.; Davies, M.B.; **Bobrick, A.** (2017)
The Astrophysical Journal Letters, Volume 851, Issue 1, (5 pp.)
- II **Faint rapid red transients from Neutron star - CO white-dwarf mergers.**
Zenati, Y.; **Bobrick, A.**; Perets, H. (2020)
MNRAS, Volume 493, Issue 3 (9 pp.)
- III **Normal type Ia supernovae from disruptions of hybrid He-CO white-dwarfs by CO white-dwarfs.**
Perets, H.; Zenati, Y.; Toonen, S.; **Bobrick, A.** (2019)
Submitted to Nature
- IV **SN 2019ehk: A Double-Peaked Ca-rich Transient with Luminous X-ray Emission and Shock-Ionized Spectral Features.**
Jacobson-Galán, W.; Margutti, R.; Kilpatrick, C.; Hiramatsu, D.; Perets, H.; Khatami, D.; Foley, R.; Raymond, J.; Yoon, S.; **Bobrick, A.**; Zenati, Y.; Galbany, L.; Andrews, J.; Brown, P.; Cartier, R.; Coppejans, D.; Dimitriadis, G.; Dobson, M.; Hajela, A.; Howell, A.; Milisavljevic, D.; Rahman, M.; Rojas-Bravo, C.; Sand, D.; Shepherd, J.; Smartt, S.; Stacey, H.; Strohm, M.; Swift, J.; Terreran, G.; Vinko, J.; Wang, X.; Anderson, J.; Baron, E.; Berger, E.; Blanchard, P.; Burke, J.; Coulter, D.; DeMarchi, L.; DerKacy, J.; Fremling, C.; Gomez, S.; Gromadzki, M.; Hosseinzadeh, G.; Kasen, D.; Kriskovics, L.; McCully, C.; Müller-Bravo, T.; Nicholl, M.; Ordasi, A.; Pellegrino, C.; Piro, A.; Pál, A.; Ren, J.; Rest, A.; Rich, M.; Sai, H.; Sárneczky, K.; Shen, K.; Short, P.; Siebert, M.; Stauffer, C.; Szakáts, R.; Zhang, X.; Zhang, J.; Zhang, K. (2020)
The Astrophysical Journal, Volume 898, Issue 2 (51 pp.)
- V **Late-time Observations of Calcium-Rich Transient SN 2019ehk Reveal a Pure Radioactive Decay Power Source.**
Jacobson-Galán, W.; Margutti, R.; Kilpatrick, C.; Raymond, J.; Berger, E.; Blanchard, P.; **Bobrick, A.**; Foley, R.; Gomez, S.; Hosseinzadeh, G.; Milisavljevic, D.; Perets, H.; Terreran, G.; Zenati, Y. (2021)
The Astrophysical Journal Letters, Volume 908, Issue 2 (13 pp.)
- VI **Introducing Physical Warp Drives.**
Bobrick, A.; Martire, G. (2021)
Classical and Quantum Gravity, Volume 38, Issue 10 (24 pp.)

VII **Looking into the cradle of the grave: J22564-5910, a young post-merger hot subdwarf?**

Vos, J.; Pelisoli, I.; Budaj, J.; Reindl, N.; Schaffenroth, V.; **Bobrick, A.**; Geier, S.; Hermes, J.J.; Nemeth, P.; Østensen, R.; Reding, J.; Uzundag, M.; Vučković, M. (2021)

Submitted to MNRAS (15 pp.)

Popular summary

Stars commonly interact with each other. The familiar stars in the night sky may appear well-separated, permanent and immutable. In contrast, observations with telescopes show that approximately every other star in our Galaxy has a stellar partner called a binary companion. Bound together by gravitational forces, pairs of stars orbit around each other in circles and, sometimes, ellipses. The orbits of such stellar binaries are so small that we cannot see them with the naked eye.

Astronomers also believe that stars change as they grow older. Our Sun, for example, will expand as a red giant at the end of its life, becoming about two hundred times larger and likely engulfing the Earth. For stars with stellar companions, such an expansion may lead to a complex interaction in which the companion will pull the material from the surface of the expanding star and turn it into a disc. As the expanded red giant loses mass to the companion, it may ignite nuclear fuel in its core and turn into a small luminous blue star called a subdwarf B star. When young, instead, stellar binaries may fly close to other stars and interact with them in stellar nurseries called star clusters.

At the end of their lives, stars may turn into dense compact stars, such as white dwarfs, neutron stars or black holes. For example, one cubic centimetre of white dwarf material may weigh about one ton. Even then, such compact stars often have a close stellar companion. Because compact stars are frequently found in very tight orbits with periods as short as half a day, they emit gravitational waves. Emitting gravitational waves costs energy, gradually bringing the stars closer and closer over time. Eventually, tight binaries become so close that the more dense companion, for example a neutron star, starts pulling material from the surface of the less dense companion, for example a white dwarf. Such exchange of material may lead to the merger of the two stars. In this case, the white dwarf star, shredded into a disc, may reach temperatures high enough that nuclear burning will take place in the disc. Such mergers may be observed as bright transient optical events in the sky.

It is sometimes said that we live in the golden age of astronomy. The Gaia satellite has recently mapped nearly two billion stars in our Galaxy, impacting nearly every branch of astronomy. The Vera Rubin Observatory, which will become operational in the coming two years, will be detecting thousands of stellar mergers and explosions every night. The observations of the stars are done through various means, including radio waves, X-rays, neutrinos and, since recently, gravitational waves. Presently, astronomers typically observe every interacting binary in several different ways.

However, how do we know which stellar interactions we are observing when we see them? A good way to answer this question is by making detailed models of interacting stars, usually with a computer, and ensuring that the predictions agree with observations. Such predictions, eventually, should reproduce all the types of observations available about the binaries. On the other hand, performing detailed simulations involves dealing with uncertainties about our models and, sometimes, with quite significant computational demands for detailed experiments. Presently, we are only starting to make such detailed comparisons, and very few types of interacting binaries may be said to be fully understood.

In this thesis, we focus on modelling the interactions of giant and compact stars. In Bobrick et al. (2017) (Paper I), for example, we study, through the use of three-dimensional hydrodynamic simulations, how white dwarfs and neutron stars interact, this way predicting whether they will merge or not. In Bobrick et al. (2021b) (Paper III), we modelled how mergers of white dwarfs and neutron stars may be observed as transient optical events in the sky, finding that they likely have been observed already. In Vos et al. (2020) (Paper II), we studied how the outcomes of interactions in red giants can tell us about the history of our Galaxy. And in Bobrick et al. (2021a) (Paper IV), we modelled how mergers of massive stars may produce stars visible to the naked eye, such as Betelgeuse.

Populärvetenskaplig sammanfattning

Stjärnor växelverkar ofta med varandra. På natthimlen kan välbekanta stjärnor förefalla väl åtskilda och beständigt oföränderliga. Emellertid visar observationer med teleskop att ungefär varannan stjärna i vår galax, Vintergatan, har en följeslagare med vilken den bildar ett dubbelstjärnsystem. Hopknutna med gravitationskrafter kretsar paren av stjärnor kring varandra i cirklar eller ibland ellipser. Banornas utsträckning för sådana dubbelstjärnor är dock så liten att vi inte kan upplösa dem med blotta ögat.

Astronomer menar att stjärnor förändras när de blir äldre. Till exempel kommer vår sol att växa till en röd jätte mot slutet av sitt liv, bli cirka tvåhundra gånger större och troligen sluka jorden. För stjärnor som har en annan som följeslagare, kan en sådan expansion leda till en komplex växelverkan där den andra stjärnan drar till sig materia från den expanderande stjärnans yta och därav bildar en skiva. När den expanderade röda jätten förlorar massa till följeslagaren kan den antända kärnbränsle i sin kärna och utvecklas till en liten lysande blå stjärna, en så kallad subdvärg av spektralklassen B. När stjärnorna är unga kan istället dubbelstjärnor råka flyga nära andra stjärnor och växelverka med dessa inuti täta stjärnhopar, platser där nya stjärnor föds.

Mot slutet av sina liv kan stjärnor utvecklas till kompakta objekt med hög täthet, såsom vita dvärgar, neutronstjärnor eller svarta hål. Exempelvis kan en kubikcentimeter av material från en vit dvärgstjärna väga cirka ett ton. Även då har sådana kompakta stjärnor ofta en följeslagare i närheten. Eftersom kompakta stjärnor ofta rör sig i mycket snäva banor med perioder så korta som bara en halv dag, avger de gravitationsvågor. Att sända ut gravitationsvågor kostar energi, och därför kommer stjärnorna med tiden gradvis att närma sig varandra. Så småningom blir banorna så snäva att den tätaste följeslagaren, till exempel en neutronstjärna, börjar dra till sig material från ytan av den mindre täta följeslagaren, kanske en vit dvärg. Ett sådant utbyte av materia kan leda till en sammansmältning av de bägge stjärnorna. I detta fall kan den vita dvärgstjärnan, som nu förvridits till en skiva, nå temperaturer som är tillräckligt höga för att kärnförbränning kan ske i skivan. På himlen kan sådana sammansmältningar observeras som snabba och ljusa uppfammanden i synligt ljus.

Ibland sägs att vi lever i astronomins guldålder. Gaia-satelliten har nyligen kartlagt nästan två miljarder stjärnor i vår galax, vilket berör nästan alla av astronomins grenar. Det förväntas att Vera-Rubin-observatoriet, som tas i drift de närmsta åren, varje natt kommer att upptäcka tusentals av stjärnors sammansmältningar och explosioner. Observationerna görs på skilda sätt, däribland med ra-

diovågor, röntgenstrålning, neutriner och sedan nyligen även med gravitationsvågor. Oftast observerar astronomer varje växelverkande dubbelstjärna på flera olika sätt.

Hur vet vi vad det är för växelverkan som vi faktiskt observerar? Ett bra sätt att svara på frågan är att utnyttja detaljerade modeller av växelverkande stjärnor, vanligen genomförda på en dator, och se till att förutsägelseerna överensstämmer med observationerna. Sådana modeller bör så småningom kunna beskriva alla typer av dubbelstjärnors observationer. Å andra sidan fordrar genomförandet av detaljerade simuleringar hantering av modellernas osäkerheter och utförliga experiment kräver ibland ganska betydande beräkningskapacitet. Ännu har vi bara precis kunnat påbörja sådana detaljerade jämförelser och mycket få typer av växelverkande dubbelstjärnor kan sägas vara helt förstådda.

I denna avhandling fokuserar vi på att modellera växelverkan mellan jättestjärnor och kompakta objekt. I Bobrick et al. (2017) (Paper I) studerar vi till exempel, genom användning av tredimensionella hydrodynamiska simuleringar, hur vita dvärgar och neutronstjärnor växelverkar. Härigenom kan vi förutsäga huruvida de kommer att smälta samman eller inte. I Bobrick et al. (2021b) (Paper III) modellerade vi hur sammansmältningen av vita dvärgar och neutronstjärnor skulle kunna observeras på himlen som kortvariga optiska skeenden och finner att de troligen redan har observerats. I Vos et al. (2020) (Paper II) studerade vi hur resultatet av växelverkan i röda jättestjärnor kan berätta om historien för vår galax. Slutligen använde vi Bobrick et al. (2021a) (Paper IV) för att modellera hur sammansmältningen av massiva stjärnor kan skapa stjärnor som blir synliga för blotta ögat, såsom Betelgeuse.

Acknowledgements

The studies in this thesis came to be through the work with four very different groups of astronomers.

I met Melvyn B. Davies and Ross Church in Lund. Thanks to them, I owe my interest in general astrophysics and some of the most valued collaborations with other people. I met Joris Vos and Maja Vuckovic at a conference in Cambridge in 2016. It felt very humbling to be so appreciated by these two astronomers, both brilliant and wonderful human beings. Our discussions might have well been the most interesting ones I had so far, as sdB stars are truly a window into binary stellar evolution. The third group, chronologically, is led by Hagai Perets at Technion. We connected thanks to serendipity and Yossef Zenati, an unconventionally excellent young astronomer. Hagai Perets group has always felt to me like the creativity centre of the world and has left me impressed for being strong, diverse and humane at the same time. Finally, my collaboration with Roberto Raddi and Manos Chatzopoulos has felt like doing astrophysics with a group of good friends who have known each other for years and years. In reality, of course, we had met relatively recently. There are many other astrophysicists and scientists whom I greatly appreciate and thank for the inspiration and numerous discussions. Special thanks go to Gianni Martire, from whom I learnt that a good way of thinking about astrophysics is in terms of startups and that diversifying (in this case, science) is the fastest way to scale.

On the side of life, I have way too many people to thank during the years, and I believe and hope they feel my gratitude. Thanks to Sara, my partner, for making the world a kind place, my parents and family, to whom I really owe the most, all my old friends, for being close despite being far, the new friends at astronomy and outside for all the great time together, the improvisation community in Malmö for making everything seem very simple and fun, and my astronomy colleagues in Lund from various times, among whom I also found good friends.

I would also like to thank the people at the Astronomy department for the strong sense of community, and who I always felt were very kind and supportive. I am grateful to the people at the Astronomy, Theoretical Physics and Physics departments and Frank Fredriksson in Ängelholm for the opportunity to teach. It had been a fantastic experience to work with many of you.

Finally, I thank my supervisor Melvyn B. Davies for the Universe, or at least a fascinating mental picture of it, for all the support and a book worth of astronomy and life lessons that have helped me greatly.

Interacting Giants and Compact Stars

Foreword

This thesis is about stellar interactions. Stars do not exist in isolation and often interact with other stars and their environment in various ways. Stars in binaries may interact by exchanging mass or merging. Stars in clusters may interact with each other through encounters and complex few-body scatterings. Exotic compact stars may merge and produce explosive supernova-like events. The four papers contained in this thesis show the diversity of possible stellar interactions.

In our first paper, Bobrick et al. (2017) (Paper I), we studied the interactions in compact white dwarf - neutron star binaries (WD-NS binaries). WD-NS binaries form detached, and a fraction of them spirals into contact due to gravitational-wave (GW) emission. In this study, we used the three-dimensional hydrodynamics code Oil-on-Water, to model how WD-NS binaries interact when they come into contact. The early interaction phase happens at very high mass transfer rates, exceeding the so-called Eddington rates by several orders of magnitude, leading to material loss. Our simulations showed that the ejected material efficiently carries away a significant amount of angular momentum in WD-NS binaries, driving them to merge. We then used the measured angular momentum in a long-term evolutionary code, and this way predicted that most WD-NS binaries will end up in a merger where the WD is tidally shredded by the NS, except for the binaries with low-mass helium WDs. As we showed in the paper, and as was confirmed by population studies later, e.g. Toonen et al. (2018), this picture agrees well with the observations of ultra-compact X-ray binaries (UCXBs), which are the outcomes of WD-NS binaries surviving the onset of mass transfer. In this paper, we showed that a short early phase of interactions may sometimes determine the further evo-

lution of binaries.

Our second paper, Vos et al. (2020) (Paper II), focussed on explaining the observed periods and mass ratios of long-period composite subdwarf B stars (sdB stars). Such binaries form when an evolved red giant (RG) star loses its envelope through interactions with a stellar companion and, additionally, ignites the helium in its core. Because sdB binaries form under very specific conditions and because their lifetimes are short compared to typical lifetimes of stars, they are considered to be excellent probes of interactions of red giants with their companions. The observed periods and mass ratios of long-period composite sdB binaries have been hard to explain with existing models. We used grids of detailed binary stellar evolution models based on the MESA code (Paxton et al., 2011) and a detailed model reproducing how the observations of such binaries are made. We found that in order to explain the periods and mass ratios in these binaries, one needs to account for the fact that the metallicity has been changing in the Galaxy over time. The red giants coming from the stars born when the Milky Way was young had lower, subsolar metallicities. As a result, their radii, for a given core mass, are smaller than they would be at solar metallicity. And as a result, the size of the orbit before and after mass transfer was also affected. Using a standard model of Galactic metallicity history and a standard model of binary evolution, we have been able to explain the observed relation and also predict and explain new observational correlations without explicitly tuning any free parameters. This study showed that the Galactic environment may be very important for interactions of stars.

Our third paper, Bobrick et al. (2021b) (Paper III), explores the fate of the WD-NS binaries that contain a massive WD and merge as a result of mass transfer. Such mergers occur relatively often in the Galaxy and may make up to about 20 per cent of the rate of type Ia supernovae. We performed three-dimensional hydrodynamic simulations of such mergers, modelling the process of the white dwarf being shredded into a disc. Because the WD material during the merger reaches high densities and temperatures, nuclear reactions occur in such discs. We modelled these nuclear reactions with the nuclear post-processing Torch code (Timmes et al., 2000) and found that mergers of WD-NS binaries with a massive WD produce a significant amount, up to $0.1 M_{\odot}$, of ^{56}Ni , among other elements. Therefore, one may expect that such mergers may lead to relatively bright supernova-like transients. We examined the likely lightcurves and spectra of the transients such systems may produce by using the supernova spectral synthesis code SuperNu (Wollaeger et al., 2013; Wollaeger & van Rossum, 2014). When doing this, we considered several models of how the post-merger object loses its material and

also examined all the known transients these mergers may correspond to. Among these, the most likely counterpart was found to be the faint type Ia supernovae. Similarly, we found that SN 2019kzr, recently suggested to come from a disruption of a massive WD, may only be produced by white dwarf-black hole binaries and only if additional non-nuclear energy sources are considered in the early days of the supernova. We also simulated our mergers with a two-dimensional hydrodynamics FLASH code and have found a likely reason why these binaries have been challenging to model with earlier 2D simulations. Altogether, this study is a good example of connecting a process involving relatively complex physics to observations.

In our fourth paper, Bobrick et al. (2021a) (Paper IV), we modelled how stars like Betelgeuse may form in our Galaxy. As has recently been realised, Betelgeuse is a very peculiar star, being a rapidly-spinning runaway red supergiant (RSG) that has likely experienced a merger in the recent past. As a runaway star, it moves with a velocity of more than 30 km/s relative to the local standard of rest. As a rapidly spinning star, it spins faster than most known RSGs and shows signs of rotation in its enhanced nitrogen abundance. As an outcome of a merger, it shows strong asteroseismic oscillations. We modelled the dynamical formation channel of stars like Betelgeuse recently proposed by Chatzopoulos et al. (2020). In this scenario, the progenitor binary is initially ejected due to a dynamical encounter in its parent cluster and subsequently merges on a subgiant branch, leading to a rapidly-rotating evolved outcome. We made a Monte Carlo model for the Galactic population of star clusters and dynamical stellar interactions within them. We modelled the actual interactions by using the Fewbody code (Fregeau & Rasio, 2007), which is a small N-body integrator. We then evolved the ejected stars with a custom population code, calculated the trajectories of these stars in the Galaxy and synthesised a mock observational dataset of such stars. We then compared the mock dataset to the actual dataset of binaries imported from the Simbad database (Wenger et al., 2000) and found a general agreement with the models, in particular showing that Betelgeuse is not alone in the Galaxy. This study demonstrates that even very familiar stars may have an interesting interaction history.

In the thesis summary that follows, we provide three perspectives on our papers. The first section is about the physical modelling of astrophysical processes in our papers. We show that stellar interactions typically involve diverse, sometimes complex, physics which may sometimes be very important for the evolution of stars. In the second section, we discuss the types of numerical codes we used in our studies. Even when considering our studies, one may observe that mod-

elling stellar interactions is almost always a trade-off between the level of detail (accuracy) and the number of systems one can model (coverage). In the third section, we examine the process of connecting the models to observations, both from the modelling and observational sides. While in no way general, we show that connecting models to observations may often require multiple steps and iterative studies on both theoretical and observational sides.

Lists of the key results of each of the four papers are given at the end of the thesis summary.

1 Physics of stellar interactions

In this section, we will be focussing on the physical processes driving the evolution of single and binary stars and the interactions between them.

1.1 Stellar evolution

A newborn sun-like star begins its life on the main sequence (MS). It burns the hydrogen fuel in its core for most of its life, thus evolving on the nuclear timescale, e.g. Kippenhahn et al. (2012). The main sequence lifetimes of sun-like stars vary strongly with the mass of the star and range between about 10 Gyr for stars of one solar mass and about 1 Gyr for two solar mass stars. After the hydrogen fuel in the core gets exhausted and turns into helium, the helium core contracts on a thermal timescale of several tens of Myr. During this time, the star is observed as a subgiant. Its radius increases by about a factor of three, and the star cools down and gradually becomes red. Once the helium core has contracted and become degenerate, the star starts burning its hydrogen in the shell around the core, and the envelope of the star becomes convective. The star is said to enter a red giant (RG) phase, which lasts up to several 100 Myr. During most of this phase, the star slowly expands, doing so faster towards the end of the phase, reaching peak radii of 200 – 300 R_{\odot} , as the He core grows from 0.1 – 0.2 M_{\odot} to a bit less than 0.5 M_{\odot} . Once the red giant reaches its maximum radius, its degenerate helium core ignites helium through a helium flash. The core rapidly becomes non-degenerate, and the star contracts becoming bluer, and then enters the core-helium burning phase called the horizontal branch (HB) phase. Since He burning proceeds faster than H burning, this phase lasts for 50 – 100 Myr and during this phase, the star has a radius of 10 – 20 R_{\odot} . Since the RG cores ignite at approximately similar masses, HB stars have similar luminosities of a few 100 L_{\odot} . Subsequently, the HB star extinguishes its He fuel in the core, the core contracts and the star expands, entering the asymptotic giant branch (AGB) stage that lasts several Myr. During this stage, the AGB star reaches about 30 – 50 per cent larger radii than during its RG phase. Nuclear burning, now happening in shells for both helium and hydrogen fuel, leads to thermal pulses. As a result, the star ejects its envelope, leaving behind a cooling core that eventually settles to become a carbon-oxygen white dwarf (CO WD).

In comparison, stars more massive than about 2.2 M_{\odot} ignite their helium cores on the RG branch non-degenerately (Hurley et al., 2000). Even more massive stars of above ten solar masses may start core helium burning already on the subgiant branch. They effectively skip the red giant phase, directly entering an

analogue of the HB phase and eventually evolve to become extended red supergiants (RSGs), reaching radii of about $1000 R_{\odot}$.

About 45 per cent of stars are found in binaries, i.e. pairs of stars gravitationally bound to each other (Raghavan et al., 2010). Further, 25 per cent of solar-like binaries are close binaries (Moe et al., 2019), meaning that their orbital periods are in the range between 1 and 10^4 d. Therefore, about 25 of all sun-like binaries will interact during their lifetimes, as the more massive primary star in the binary at some point will have its radius comparable to the size of the binary orbit. As we will discuss further, binary interactions may lead to a variety of outcomes that are impossible to produce through single stellar evolution, e.g. Hurley et al. (2002).

Apart from the initial mass, metallicity is the second most important parameter determining stellar evolution. Metallicity is defined as the fraction of metals (which is representative of iron) in the star compared to that in the Sun, i.e. $[Fe/H] \equiv \log_{10}(Z/Z_{\odot})$, wherein $Z_{\odot} = 0.0142$ is the solar mass fraction of elements heavier than helium (Asplund et al., 2009). The presence of metals in stars may affect their main sequence lifetimes by several Gyr. Furthermore, the close binary fraction anticorrelates with metallicity (Moe et al., 2019), implying that close binaries are more common at lower metallicity.

Even a metallicity difference of about 0.4 dex, quite typical for the Milky Way (Edvardsson et al., 1993), may affect the maximum radii of solar-mass RGs by about 20 per cent, e.g. Choi et al. (2016). The difference may be understood since higher metallicity leads to higher opacity, leading to stronger convection in RG envelopes and making them physically bigger. For a similar reason, metallicity is strongly correlated with the ability of stars to lose mass through stellar winds, e.g. Vink et al. (2001). As we discuss further, these correlations may significantly affect the lives of both massive and solar-like binary stars, e.g. Chruslinska et al. (2019), Vos et al. (2020) (Paper II).

Stars are generally born in clusters or stellar associations (Kroupa, 2001), as illustrated in Figure 1. The clusters subsequently dissolve, typically on timescales much shorter than lifetimes of sun-like stars. Such clusters, in turn, form within their environments, which may vary significantly both in terms of star formation rate and metallicity. The present-day Galaxy is a collection of stars of different masses, ages and metallicities born throughout its history. As we discuss further, modelling the populations of interacting binaries in the Galaxy may require one to take into account its history.

The lives of massive stars may differ quite significantly from their solar-like counterparts. Stars more massive than about 8 solar masses will end their lives as

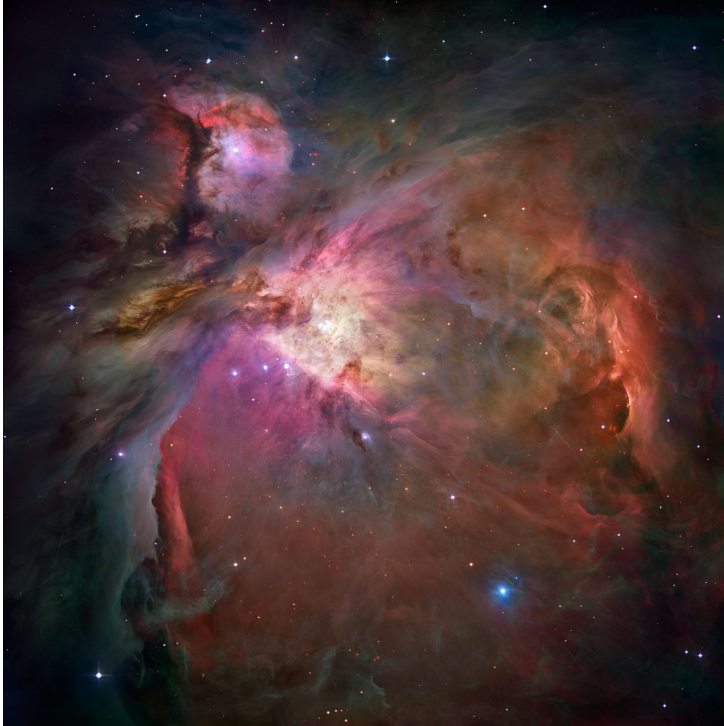


Figure 1: Hubble Space Telescope (HST) view of the Orion nebula – the closest large site of ongoing star formation in the Galaxy. The false colour composite image highlights hydrogen in orange, oxygen in green, sulfur and infrared observations in red. Nearby red supergiant Betelgeuse likely has originated in a cluster in the Orion nebula complex. Image credit: ESA, NASA.

core-collapse supernovae (CCSNe), e.g. Hurley et al. (2000). The explosion will leave behind a neutron star (NS) or a black hole (BH), typically kicked in both cases, e.g. Hobbs et al. (2005); Repetto et al. (2012). If the resulting binaries remain intact, other types of interactions may occur, e.g. Bobrick et al. (2017) (Paper I), Bobrick et al. (2021b) (Paper III), as we discuss further. Massive stars evolve much faster than low-mass stars. The typical timescales are about 100 Myr for $5 M_{\odot}$ stars, down to about 10 Myr for stars of $20 M_{\odot}$, down to a few Myr for the most massive stars. Massive stars are also rarer than their sun-like counterparts, with only about one per several hundred stars ending their life as a CCSN (Kroupa, 2001). For these reasons, there are far fewer massive stars observed compared to solar-like stars. Massive stars are also significantly windier compared to sun-like stars, which is related to their extreme luminosities. For RSGs, for example, the radiative pressure is balancing the gravitational pull of the stars, which is why RSGs have such sparse and extended envelopes.

The majority of massive stars are found in binaries or high-order multiples (Moe & Di Stefano, 2017). More than 70 per cent of massive stars will interact with a companion during their lifetimes (Sana et al., 2012). In other words, it is relatively rare for massive stars not to interact with each other.

Due to their short lifetimes, about 80 per cent of massive stars are found inside young clusters (Gvaramadze et al., 2012). Within clusters, typically containing between 10 and 10000 stars, massive stars tend to quickly sink into the core on timescales inversely proportional to their mass (Fregeau et al., 2002). The segregated massive stars then encounter each other dynamically. The preference for massive stars to interact with other massive stars may be understood because their interaction cross-section is dominated by gravitational focusing and is proportional to their mass, $\sigma \propto M$. Some of these dynamical encounters lead to ejections of single and binary massive stars from their birth environments. Such processes are common for massive stars, as we discuss further, e.g. Bobrick et al. (2021a) (Paper IV). In particular, the well-known Betelgeuse star has likely formed this way.

1.2 Mass transfer in binary stars

Roche lobe overflow (RLO) occurs when the outer parts of a star are effected by a companion's gravity, e.g. Webbink (1985). Single stars are typically bound by their own gravity. However, when in binary, each star has a Roche lobe – the region where their gravity is dominant. If outer parts of a star reach outside of its Roche lobe, they get stripped by the gravity of their companions, producing a

semi-detached binary.

RLO may occur because of stellar evolution, e.g. when one of the stars evolves to become an RG. It may also occur because the binary orbit has shrunk because of the loss of angular momentum. Gravitational waves (GWs), for example, may carry away angular momentum. GW emission takes place in compact binaries with orbits smaller than about $4 R_{\odot}$ (Peters, 1964). In particular, the emission of GWs is responsible for inspiral and mass transfer in WD-NS binaries in Bo-brick et al. (2017) (Paper I). Magnetic braking (MB) may occur in binaries with magnetic and windy MSs (e.g. MS's with a convective layer). A wind, coupled to the magnetic field of the stars, then may carry away angular momentum (Rappaport et al., 1983) and make the binary shrink. Flybys in dynamical environments, e.g. Davies (1995), tides in binaries, e.g. Hut (1981); Zahn (1975), triple stellar interactions, e.g. Toonen et al. (2016), may also cause stars to initiate the RLO.

The Roche lobe volumes of the stars in a binary, V_{RL1} and V_{RL2} , may be estimated by replacing the stars by point masses M_1 and M_2 , e.g. Kopal (1959). The condition for RLO may then be obtained by equating the volumetric radius $R_{\text{RL}} \equiv (3V_{\text{RL}}/4\pi)^{1/3}$ to the radius R_1 or R_2 of the stars. In practice, R_{RL} defined this way is calculated numerically, and it may well be approximated, for example, by Eggleton's formula (Eggleton, 1983):

$$R_{\text{RL},1} \equiv a f_{\text{RL},1}(q) = a \frac{0.49q^{2/3}}{0.6q^{2/3} + \ln(1 + q^{1/3})} \quad (1)$$

Equation 1 defines the Roche lobe radius $R_{\text{RL},1}$ as a function of semimajor axis a and binary mass ratio $q = M_1/M_2$. $R_{\text{RL},1}$ makes up about 0.3–0.4 fraction of the semimajor axis a for comparable binary masses and reaches about 0.2 for small M_1/M_2 and about 0.6 for large M_1/M_2 .

The RLO condition $R_1 = a f_{\text{RL},1}(q)$ implies that the period at Roche lobe overflow is mostly the function of the average density of the Roche lobe overflowing star, $P_{\text{RLO}} \propto \langle \rho \rangle^{-1/2}$ (Eggleton, 1983). Indeed:

$$P_{\text{RLO},1} = 2\pi \left(\frac{GM_{\text{tot}}}{a^3} \right)^{-1/2} = 2\pi \left(\frac{GM_1(1+q)f_{\text{RL},1}^3(q)}{R_1^3} \right)^{-1/2} \propto \langle \rho_1 \rangle^{-1/2} \quad (2)$$

Neglecting the mass ratio-dependent term $((1+q)f_{\text{RL},1}^3(q))^{-1/2}$ is justified because it is a weak function of q . Indeed, it varies between 0.2 for small q and 0.4 for large q . The relation between the RLO period and density is useful for estimating which of the two stars overflows its Roche lobe first. For example, it may

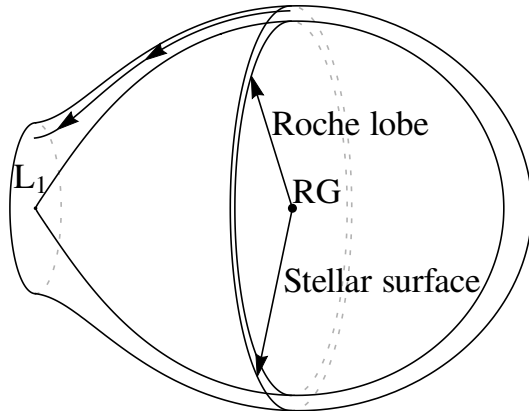


Figure 2: Structure of the mass flow from a red giant (RG) overflowing its Roche lobe. In the figure, made by the author, the outermost layers of the RG are outside of the Roche lobe surface. Being gravitationally unbound to the RG, the material from the outer layers flows towards the nozzle around the L_1 point, subsequently falling into the Roche lobe of the companion. The material flows in a steady fashion, following streamlines, which allows one to obtain mass loss rate for such systems analytically.

be readily inferred from this relation that the Earth will strip mass from the Sun when it becomes an RG and not the other way around.

Mass flow from the overflowing star may be visualised as in Figure 2. Both the surface of the star and the Roche lobe are equipotential surfaces. The outside layers of the donor star may also freely flow along the equipotential surfaces. Near the L_1 point, the donor material flows outwards into the Roche lobe of the companion. Without pressure support from a stellar surface on the other side, the material ballistically falls in to form a disc (Lubow & Shu, 1975). Shocks from self-crossings turn the energy into heat but preserve the angular momentum. The characteristic radius of the disc formed by the accreted material is called the circularisation radius and is defined through angular momentum conservation. Subsequently, the material in the outer layers of the donor is replenished from below. The material in the disc viscously spreads and leads to accretion on the companion. The viscously heated accretion disc may be observed in X-rays, as is the case with NS/BH

accretors, e.g. Savonije et al. (1986), in soft X-rays and UV's for WD accretors, e.g. in CV's (Faulkner, 1971) or symbiotic binaries (Kenyon, 1986), and in UV's or optical bands for low-mass MS accretors (Fujimoto et al., 1981).

Ritter's formula (Ritter, 1988) expresses \dot{M} of the donor star through the depth of the Roche lobe inside it, $\Delta R = R_1 - R_{\text{RL},1}$, which is also called sometimes the degree of overflow:

$$\dot{M} \propto e^{\Delta R/h_P} \quad (3)$$

In the equation, h_P is the pressure scale height of the atmosphere of the donor. We can see that the mass transfer (MT) rate is a sensitive function of how deeply does the Roche lobe dig into the donor star. Formula 3 applies to MT from above the photosphere, where the temperature may be assumed to be constant and equal to the effective temperature T_{eff} , while the gas may be treated as ideal. The formula may be derived by remembering that $\dot{M} = \int \rho_{\text{L1}} v_{\text{L1}} dA_{\text{L1}}$, where the integration is taken over the nozzle centered on the L_1 point:

$$\dot{M} = \int_0^{\Delta R} \rho_{\text{L1}}(r_{\text{L1}}) v_{\text{L1}}(r_{\text{L1}}) 2\pi r_{\text{L1}} dr_{\text{L1}} \quad (4)$$

In the above expression, r_{L1} is the distance from the L_1 point. This distance may be expressed through the radius $r = R_{\text{RL},1} + r_{\text{L1}}$ in the star from which the streamline starts. Furthermore, the velocity through the nozzle is equal to the sound speed, $v_{\text{L1}}(r) = c_s = \sqrt{\gamma \mathcal{R} T_{\text{eff}} / \mu}$, where γ is the adiabatic constant, μ is the molar mass and \mathcal{R} is the gas constant (Lubow & Shu, 1975). This result may be understood because the gas crossing the nozzle expands effectively into empty space with the gas acquiring characteristic molecular velocities, which are close to the sound speed. Finally, one may calculate the $\rho_{\text{L1}}(r_{\text{L1}})$ term from the Bernoulli equation applied to the streamline and assuming that along the streamline, the expansion is adiabatic, $P \propto \rho^\gamma$:

$$\frac{P}{\rho} + \frac{v^2}{2} = \text{const} \quad (5)$$

At the location where the streamlines start, i.e. deep inside the stellar atmosphere, the velocity v of the fluid is close to zero compared to the speed of sound. Therefore, we can express the properties at the ends of the streamlines as:

$$\frac{P}{\rho} = \frac{P_{\text{L1}}}{\rho_{\text{L1}}} + \frac{c_s^2}{2} \quad (6)$$

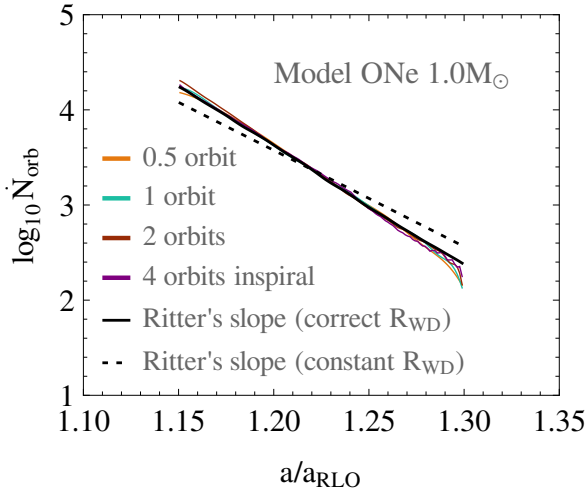


Figure 3: Numerical verification for the Ritter’s formula, based on mass transfer modelling in a $1 + 1.4 M_{\odot}$ ONe WD-NS from Bobrick et al. (2017) (Paper I). The thick black line shows the analytical prediction for mass transfer rate \dot{M} versus binary separation a . The solid line accounts for the change of the volumetric radius of the donor WD with separation, while the dashed line assumes a constant radius. The thin lines are the results of numerical experiments.

Furthermore, for the speed of sound, we may write $c_s^2 = (\partial P / \partial \rho)|_S = \gamma P / \rho$. This way, one may arrive at the expression connecting the density near the nozzle and in the atmosphere, $\rho_{L,1}(r_{L1}) \propto \rho(R_{RL,1} + r_{L1})$. Finally, for ideal gas atmospheres, $\rho(R_{RL,1} + r_{L1}) = \rho_0 \exp(-r_{L1}/h_P)$. As a result, to the leading order in the degree of overflow ΔR :

$$\dot{M} \propto \rho_0(R_{RL,1}) \int_0^{\infty} \exp(-r_{L1}/h_P) r_{L1} dr_{L1} \propto \rho_0(R_{RL,1}) \propto e^{\Delta R/h_P} \quad (7)$$

The Roche lobe may also be located below the photosphere, and T_{eff} and h_P may be changing with depth. For this case, a more general Kolb & Ritter (1990) prescription applies. Recently, Ritter’s formula has been verified numerically through hydrodynamic simulations by Bobrick et al. (2017) (Paper I), as we show in Figure 3. It is worth remembering that the interaction of the two stars is not the same as for point masses. Quadrupolar terms from the mass distribution affect the orbital frequency Ω , and correspondingly, the Roche lobe, by a few per cent (Bobrick et al., 2017) (Paper I). The stars also do not exactly preserve their

volume when deformed and increase in their volumetric radius by a few per cent, and even up to ten per cent for comparable-mass binaries (Bobrick et al., 2017) (Paper I). In the case of AGB (Abate et al., 2013) or massive stars (El Mellah et al., 2019), there may occur intermediate cases of wind-RLO when wind mass transfer interplays with the gravity of the binary. Finally, at high mass transfer rates, MT also may occur through the L_3 point behind the donor (Pavlovskii et al., 2017).

As follows from Equation 3, MT is affected both by the orbit and the depth of the Roche lobe inside the donor. One may notice, in particular, that MT can only start gradually, starting from zero. This phase is called the onset phase of mass transfer. The onset of MT always starts on a timescale given by

$$\tau_{\text{MT}} = \frac{\dot{M}}{\ddot{M}} = \frac{h_P}{R} \frac{R}{\dot{R}} \propto \frac{h_P}{R} \tau_E \quad (8)$$

where τ_E is the timescale of the evolutionary process leading to mass transfer. Therefore, stars with thin atmospheres, for example, WDs, may initiate mass transfer very quickly. WDs may have h_P/R of about 10^{-5} , and while their GW timescales may be of the order of 1 kyr for the case of a $1.4 + 0.6$ WD-NS binary (Peters, 1964), their MT onset happens on the timescale of days. As the Roche lobe digs deeper than the photosphere, the onset slows down, but only to a small extent.

Since MT grows on a short timescale, we expect it to become significant and provide feedback onto the orbit quickly, e.g. Webbink (1985). Secular evolution equations describe what happens to MT and the binary over timescales much longer than the orbital period P . We can derive these equations by assuming circular orbits, and log-differentiating the equation for the angular momentum of the binary, $J_z = \sqrt{GM_1^2 M_2^2 a / (M_1 + M_2)}$:

$$\frac{\dot{J}_z}{J_z} = \frac{\dot{M}_1}{M_1} + \frac{\dot{M}_2}{M_2} - \frac{1}{2} \frac{\dot{M}_1 + \dot{M}_2}{M_1 + M_2} + \frac{1}{2} \frac{\dot{a}}{a} \quad (9)$$

This equation may be solved by reducing the number of independent variables. For example, we may assume that the accretor captures a certain fraction β of the mass lost by the donor, $\dot{M}_2 = -\beta \dot{M}_1$. We may also expect that the parameter β varies much slower than the mass transfer rate \dot{M} . Furthermore, since the binary angular momentum is intrinsically conserved, it may change only due to external angular momentum loss processes $\dot{J}_z/J_z = -\left(\dot{J}_z/J_z\right)_{\text{loss}}$, which may include the effect of GWs, MB, tides, spins and other processes. Finally, we also can

express the binary semimajor axis through the Roche lobe radius through $a = R_{\text{RL},1}/f_{\text{RL},1}(q)$. Hence:

$$\frac{\dot{a}}{a} = -\frac{\Delta\dot{R}}{R_1} + \frac{\dot{R}_1}{R_1} - \frac{f'_{\text{RL},1}}{f_{\text{RL},1}} \left(\frac{\dot{M}_1}{M_2} - \frac{M_1\dot{M}_2}{M_2^2} \right) \quad (10)$$

We may then adopt mass-radius exponent ζ_1 defined as

$$\frac{\dot{R}_1}{R_1} \equiv \zeta_1 \frac{\dot{M}_1}{M_1} + \left(\frac{\dot{R}_1}{R_1} \right)_{\text{evol}} \quad (11)$$

and the Roche-lobe parameter $\zeta_{\text{RL}} \equiv qf'_{\text{RL},1}/f_{\text{RL},1}$. Combining all the \dot{M}_1 terms in Equation 9 together, we arrive at the secular evolution equation for mass transfer:

$$\frac{\Delta\dot{R}}{R_1} = 2 \left(\frac{\dot{J}_z}{J_z} \right)_{\text{loss}} + \left(\frac{\dot{R}_1}{R_1} \right)_{\text{evol}} + X \frac{\dot{M}_1}{M_1} \quad (12)$$

In the above equation:

$$X = 2(1 - \beta q) - (1 - \beta)q/(1 + q) + \zeta_1 - \zeta_{\text{RL}}(1 + \beta q) \quad (13)$$

X is a slowly-varying parameter of order unity. Formally, one may obtain the evolution of the mass transfer rate by solving Equation 12 together with equation for $\dot{M}_1(\Delta R)$, such as the Ritter's formula 3.

We saw earlier that mass transfer rate \dot{M} is a sensitive function of the degree of overflow ΔR . From the secular evolution equation, we see that a constant angular momentum loss, e.g. due to GWs or MB, generally pushes the system towards shrinking, increasing the degree of overflow ΔR and, correspondingly, \dot{M} . Similarly, if evolution causes the stellar radius to expand, it will push towards higher ΔR and \dot{M} . Eventually, the last term in Equation 12, proportional to \dot{M} , becomes so large that it becomes comparable to the J_z loss term. At this point, mass transfer starts depending on mass transfer itself. The subsequent evolution then is strongly dependent on the values of the parameter X .

Earlier, we assumed that the accreting star only accreted a fraction β of the mass lost by the donor. Therefore, we assumed that the system as a whole loses mass at a rate of $\dot{M}_{\text{lost}} = (1 - \beta)(-\dot{M}_1) \geq 0$. The lost mass also carries away angular momentum, which we parametrize as $\dot{J}_{z,\text{loss,MT}} = \alpha(J_z/\mu)\dot{M}_{\text{lost}}$, where $\mu \equiv M_1 M_2 / (M_1 + M_2)$. Therefore:

$$\left(\frac{\dot{J}_z}{J_z} \right)_{\text{loss,MT}} = \alpha(1 - \beta)(1 + q) \frac{-\dot{M}_1}{M_1} \quad (14)$$

Physically, the angular momentum carried away from the system by mass loss also drives the system towards increasing its mass transfer rate \dot{M} . Importantly, because in Equation 14, J_z loss is proportional to \dot{M} , this effect becomes even more significant at the end of the onset when the \dot{M} term starts dominating MT.

The parameter α may take a range of values. It may even dominate MT depending on how exactly material is lost from the binary. In binary population modelling, there are four parameters commonly used to describe mass and angular momentum loss: $\bar{\alpha}$, $\bar{\beta}$, $\bar{\delta}$ and $\bar{\gamma}$ (van den Heuvel, 1994; Soberman et al., 1997). Parameter $\bar{\alpha}$ describes mass loss from the donor in the form of a fast wind. Parameter $\bar{\beta}$ describes mass loss through a jet from the vicinity of the accretor. Parameter $\bar{\delta}$ corresponds to mass loss from a circumbinary toroid, with parameter $\bar{\gamma}$ corresponding to the radius of the toroid in units of $\sqrt{a_{\text{toroid}}/a}$, effectively encoding the angular momentum content in such toroid, see e.g. Tauris & van den Heuvel (2006). In our notation, $\beta = 1 - \bar{\alpha} - \bar{\beta} - \bar{\delta}$, and α is given by:

$$\alpha(1 - \beta) = \frac{\bar{\alpha}}{(1 + q)^2} + \left(\frac{q}{1 + q}\right)^2 \bar{\beta} + \bar{\gamma}\bar{\delta} \quad (15)$$

While parameters $\bar{\alpha}$, $\bar{\beta}$, $\bar{\delta}$ and $\bar{\gamma}$ are derived from somewhat idealised physical scenarios, it may be seen that $\alpha(1 - \beta)$ term in Equation 12 may easily be of order unity, this way significantly modifying parameter X .

Complex physics often governs realistic mass loss. As an example, consider a sun-like MS star accreting through RLO. Accretion of even $0.01 M_{\odot}$ of material spins up the central star to critical velocities (Popham & Narayan, 1991). While the star may lose some angular momentum through viscous or magnetic torques, it cannot do it efficiently if the accretion is ongoing (Popham & Narayan, 1991; Paczynski, 1991; Deschamps et al., 2013). This pile-up of material prevents further accretion, making the binary lose mass. For example, in our detailed stellar structure modelling in Vos et al. (2020) (Paper II), we found that in RG-MS mass transfer, MS stars reach over-spinning at $\dot{M} \geq 10^{-5} - 10^{-6} M_{\odot}/\text{yr}$. Accreting MS stars also may lose mass because of swelling due to accretion. The material newly landing onto the surface of an MS star releases gravitational energy into heat, this way depositing heat on the surface. If the thermal timescale for the star is longer than the timescale of mass transfer, the accretor starts swelling (Kippenhahn & Meyer-Hofmeister, 1977; Pols & Marinus, 1994; Toonen et al., 2012). In Vos et al. (2020) (Paper II), we found that over-spinning for MS accretors typically takes place earlier than swelling.

Similar effects of over-spinning and swelling may, in principle, also affect WD and NS accretors, depending on their ability to spin down or cool down. The

process is further complicated by the possibility of nova and X-ray bursts, which may also carry away mass and angular momentum even if the material could get accreted otherwise, e.g. Nomoto et al. (1984); Iaria et al. (2021). For WDs and especially NSs, the radiation pressure from the accretion luminosity may additionally prevent accretion. For an accreting mass, the Eddington luminosity is given by

$$\dot{M}_{\text{Edd}} = 2.1 \cdot 10^{-8} \frac{\eta}{0.15} \frac{M_2}{1.4 M_{\odot}} M_{\odot}/\text{yr} \quad (16)$$

where η is the accretion efficiency (Cameron & Mock, 1967; Hurley et al., 2002). The expression shows that one may expect NS's to be non-conservative even at relatively low mass transfer rates.

The secular evolution Equation 12 leads to two qualitative solutions. If MT rate stabilizes and changes on the timescale driving the evolution initially, the case is called stable MT. From Ritter's formula 3, we see that

$$\frac{\Delta \dot{R}}{R_1} = \frac{h_P}{R_1} \frac{\dot{M}_1}{\dot{M}_1} \quad (17)$$

If the timescale of MT evolution becomes comparable to the timescale driving the evolution, the term $\Delta \dot{R}/R_1$ vanishes due to $h_P/R_1 \ll 1$ factor. The equation for stable MT evolution then becomes:

$$\frac{\dot{M}_1}{M_1} (X - 2(1+q)(1-\beta)\alpha) = -2 \left(\frac{\dot{J}_z}{J_z} \right)_{\text{loss,not MT}} - \left(\frac{\dot{R}_1}{R_1} \right)_{\text{evol}} \quad (18)$$

We see that indeed mass transfer is happening on the timescale driving the evolution, so long as:

$$X - 2(1+q)(1-\beta)\alpha_{\text{loss}} > 0 \quad (19)$$

Expression 19 is called the MT stability condition. It needs to be satisfied for MT to be stable. We see that large q for non-conservative systems makes it difficult for them to satisfy the condition. Also, for non-conservative systems, the parameters of non-conservative MT, α and β , may change the evolution timescale by a factor of several, especially if $X - 2(1+q)(1-\beta)\alpha$ is close to zero.

Equation 18 may be integrated analytically. Indeed, on the left-hand side, since

$$\frac{\dot{q}}{q} = \frac{\dot{M}_1}{M_1} - \frac{\dot{M}_2}{M_2} = \frac{\dot{M}_1}{M_1} (1 + \beta q) \quad (20)$$

there is a function of q only. Assuming, for example, that mass transfer is driven by evolution alone, one may obtain:

$$\frac{R_{\text{fin}}}{R_{\text{init}}} = \exp \left(- \int_{q_{\text{init}}}^{q_{\text{fin}}} \frac{X - 2(1+q)(1-\beta)\alpha}{q(1+\beta q)} dq \right) \quad (21)$$

Such considerations may be applied when one knows the final mass of the donor at the end of MT. For example, in the case of RG mass transfer, one may expect that the final mass of the donor may be approximately equal to the core mass of the RG. Therefore, one may analytically estimate the orbits of the binaries after the RG envelope has been lost. One may apply a similar derivation for stable MT driven by GWs, although one would have to integrate masses on the left-hand side instead of mass ratios.

In the unstable MT case, when condition 19 is not satisfied, the onset of mass transfer does not end when the MT timescale becomes comparable to that of the driving process. As a result of the continued growth of mass transfer rate, the secular evolution equation becomes:

$$\frac{h_P}{R} \frac{\ddot{M}_1}{\dot{M}_1} = X \frac{\dot{M}_1}{M_1} \quad (22)$$

One may obtain the solution for this equation by assuming X and R constant, which gives, to the lowest order in h_P , $-\dot{M}_1 = (-X)^{-1}(h_P/R)M_1/(t_{\text{fin}} - t)$. In the case of a giant donor, such unstable evolution leads to the system evolving on a dynamical timescale and undergoing a common envelope episode, e.g. Webbink (1985); Ivanova et al. (2013). The core and the companion star, in this case, spiral into the envelope, eventually ejecting it or merging. In the case of non-giant stars, unstable mass transfer may produce merged objects, as is the case for WD-NS binaries with massive WD companions (Bobrick et al., 2017) (Paper I), (Bobrick et al., 2021b) (Paper III).

Stellar evolution also proceeds during mass transfer. For example, Sengar et al. (2017) showed that subgiants and early red giants may overflow their Roche lobe, transfer mass to an NS companion, and evolve into a He WD-NS binary without detaching. An even stronger example is the formation of sdB-MS binaries (Han et al., 2002, 2003; Heber, 2009). In this case, the RG initiates mass transfer while still having a degenerate core. However, during or right after mass transfer, the core ignites He and undergoes a He flash. A similar situation may happen in, for example, mass-transferring He Star-NS binaries (Rappaport et al., 1982; Nelson et al., 1986; Podsiadlowski et al., 2002). In this case, the donor undergoes nuclear

burning and changes its composition directly during stable mass transfer. For this reason, the evolution of some binaries through mass transfer needs to be modelled through the use of detailed stellar structure codes.

Even assuming that the evolution of the donor has been modelled in detail, its appearance right after MT may differ significantly from that expected from an idealised isolated version of the donor remnant. For example, RG-NS MT may leave behind a He WD. However, even from single stellar evolution (e.g. Hurley et al., 2000; Kippenhahn et al., 2012), we know that AGBs first produce hot pre-WDs, which have to follow the cooling track to become WDs. During such evolution, the pre-WD radius may exceed the radius of the cold WD by a factor of several. Recently, Istrate et al. (2014, 2016) showed that for low-mass He WDs of $\lesssim 0.2 M_{\odot}$ resulting from subgiant and giant mass transfer, such a phase may last for longer than 1 Gyr. Such early phases may be important both for observations of such systems and the possible subsequent binary interactions.

Even finer details are important for observations. For example, consider possible outcomes of RG mass transfer. If the RG detaches, having transferred very little material, it will follow the evolution of an HB star. If an RG loses all of its envelope and still ignites the core, it will be observed as an sdB star. Such stars are blue and lack hydrogen in their spectra (Heber, 2009). If the RG retains some envelope, $> 0.02 M_{\odot}$, the envelope will make the sdB star appear redder. As a result, it will be classified as an sdA star. If a He WD is produced, the residual envelope may also affect its classification. The exact amount of envelope left on the core He-burning star may also be important for evolution. For example, an HB with an extended envelope may evolve into a much larger giant than an sdB star. Whether the core ignites helium and the amount of envelope left on the donor must be studied with detailed stellar structure codes.

sdB stars are excellent laboratories of mass transfer. The main reason is that they live only about 100 Myr and form under very specific conditions. In particular, for a given progenitor mass M_1 , only a relatively narrow range of companion masses M_2 may lead to the formation of sdB stars. Therefore, by spectroscopically determining the companion mass, one may infer the initial progenitor mass. Furthermore, the final periods of long-period sdBs are mainly sensitive to the donor metallicity and the initial orbital periods (Vos et al., 2020) (Paper II). Therefore, by observations of the present long-period sdB population, one may reconstruct which original binaries produced them.

One important application of sdB stars to stellar evolution is that their final mass ratios are sensitive to the assumptions about the conservativeness of mass

transfer. The observed dataset of sdB stars requires unambiguously that MS accretors with $M < 1.5 M_{\odot}$ can only accrete mostly non-conservatively for $\dot{M} > 10^{-5} M_{\odot}/\text{yr}$ (Vos et al., 2020) (Paper II). This conclusion is further supported by the low rotation rates and abundances of the companions (Vos et al., 2018), as we discuss further. The result is also consistent with the earlier discussion that MS stars likely are unable to accrete at $\dot{M} > 10^{-5} M_{\odot}/\text{yr}$ due to over-spinning and swelling. The conclusion, however, is important for any stellar modelling of post-RG-MT stars.

Similarly, since the orbits of sdB stars are sensitive to their initial periods, they put constraints on their progenitors. The range of final periods may be turned into constraints on the range of RG radii that experienced MT. Since the progenitor mass is sensitive to age, which is sensitive to metallicity and since metallicity also affects the RG radii, there is a correlation between the progenitor mass and radii. As it turns out, the effect of Galactic metallicity on radii is necessary to account for when modelling the orbits of the observed sdBs (Vos et al., 2020) (Paper II). This fact shows, in particular, that even such details as the initial metallicity may be in some cases crucial in explaining the present-day properties of interacting binaries. Metallicity also plays a very important role in producing GW sources, such as DBH, BH-NS or DNS binaries, e.g. Chruslinska et al. (2019). In this case, metallicity affects the formation rates both through its effect on giant radii and the ability of massive stars to lose mass into the winds.

1.3 Detailed physics of mass transfer

In this section, we discuss examples of systems for which detailed physics of mass transfer is important.

As we discussed earlier, the mass transfer process starts with the onset from very low MT rates. Then it either brings the system to a stable MT regime when \dot{M} switches from the rapid evolution on timescales $\sim (h_P/R)\tau_{\text{evol}}$ to a slower evolution on the MT-driving timescales τ_E . Alternatively, unstably-transferring systems keep on evolving on short timescales towards instability.

In all these cases, the mass transfer rate \dot{M} changes over many orders of magnitude. Therefore, it is natural to expect that different physics governs mass loss depending on the mass transfer rate. For example, let us focus on red giant mass transfer. In the limit of very low MT rates, the disc is optically thin, cannot cool down efficiently, and is geometrically thick (Shakura & Sunyaev, 1973). At somewhat more moderate rates of above $10^{-10} M_{\odot}/\text{yr}$, the accretion onto MS stars may proceed through a geometrically-thin disc and, not impeded by the ac-

cretor swelling and over-spinning, may perhaps be conservative. At rates above $\dot{M} > 10^{-5} M_{\odot}/\text{yr}$, sun-like MS stars cannot accept mass efficiently. However, even then, it is not fully clear how exactly mass gets ejected from the system. The material may get lost through a jet or an outflow, e.g. Tauris & van den Heuvel (2006) and Shiber & Soker (2018), or it may fill the Roche lobe of the accretor and perhaps get ejected isotropically, as seen in symbiotic systems (Munari, 2019). At yet higher MT rates of about $10^{-3} - 10^{-4} M_{\odot}/\text{yr}$ an additional L_2 mass loss in the orbital plane likely becomes important (Pejcha et al., 2017). Subsequently, at $10^{-2} M_{\odot}/\text{yr}$ also L_3 mass loss from behind the donor occurs, also in the orbital plane (Pavlovskii et al., 2017). RG-MS systems reaching such rates may remain stable and avoid a CE episode (Bobrick et al. in prep). The different geometries of mass loss (spherical/conical/planar) are reflected in the shapes of observed pre-planetary nebulae (Jones & Boffin, 2017). Yet, there is no unambiguous identification so far between the regimes of mass loss and mass transfer rates in RG-MS binaries. It should be added that long-period sdB binaries, while being very good probes of mass transfer, are relatively insensitive to the angular momentum loss (Rappaport et al., 1995; Chen et al., 2013). The lack of such sensitivity is related to the fact that sdB formation is sensitive to the conditions in the RG at the end of mass transfer. Different geometries of mass loss most certainly affect the angular momentum content of the lost material and may, in principle, be important for some binary populations.

For WD-NS binaries, the range of mass transfer rates may be even higher, as we show in Figure 4 from Bobrick et al. (2017) (Paper I). If WD-NS binaries could eject mass only through a jetted-outflow, as they do in X-ray binaries, massive CO WDs would be able to reach rates of millions of times higher than the Eddington rate and remain stable (van Haften et al., 2012). While we observe ultraluminous X-ray sources (Kaaret et al., 2017) with MT rates of a few 100 times above Eddington (assuming they are radiating isotropically), it is very likely that the regime of mass loss in binaries transferring at hundreds of times higher rates is different. The jet-showing X-ray binaries are typically sub-Eddington (Casares et al., 2017). The observed SS 433 system, for example, is super-Eddington and shows disc outflows and a jet (Cherepashchuk et al., 2020), which motivates our phase 3 of mass loss in the figure. For the higher, Eddington-dominated, mass transfer rates, we have performed simulations with an Oil-on-Water code adopted to this regime (Bobrick et al., 2017) (Paper I), i.e. wherein the NS accretor is set not to accrete any material. We found that the material is ejected before it reaches the vicinity of the accretor. By the ejection time, it contains much more angular

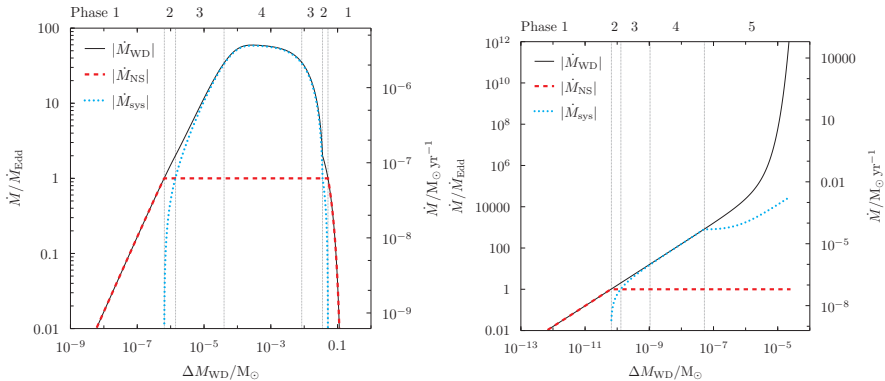


Figure 4: Evolution of mass transfer rate for WD-NS binaries with a $0.15 M_{\odot}$ WD and a $1.4 M_{\odot}$ NS (left panel) and a $0.75 M_{\odot}$ WD and a $1.4 M_{\odot}$ NS (right panel) showing, correspondingly, an example of stable and unstable evolution. The regime of mass loss changes depending on the mass transfer rate from the WD. Phase 1 corresponds to conservative mass transfer. Phase 2 corresponds to the mass loss through a collimated jet. Phase 3 corresponds to mass loss through a collimated jet and a disc wind. Finally, phase 4 corresponds to mass loss through a pure disc wind choking the jet. This figure is from Bobrick et al. (2017) (Paper I).

momentum than the accretor itself. As the disc wind leaves the binary, the binary deposits additional torque into the wind, losing a further amount of angular momentum. An important physical point that followed from this study is that to infer what happens to mass flow in the super-Eddington regime when the accretor cannot take mass in, one needs to investigate the global structure of the disc rather than the immediate vicinity of the accretor. While the material pile-up does start near the accretor, the pile-up effects can quickly become system-wide.

The evolution sequence for most WD-NS binaries is that the onset of mass transfer initially happens on timescales of days to years, depending on the WD mass. Then, the binary enters a lossy regime, initially with a jet, later with a wind outflow. Then the binary enters a highly super-Eddington regime. This regime leads to a strong angular momentum loss. This angular momentum loss drives many binaries to instability. If one were to ignore the correct angular momentum loss during this phase, MT would have been stable. Nevertheless, in reality, only WD-NS binaries with low-mass He WDs with $M_{\text{wd}} < 0.2 - 0.3 M_{\odot}$ survive the onset. The unstably transferring binaries merge on similar timescales producing a transient event (Zenati et al., 2020), (Bobrick et al., 2021b) (Paper III). The stably transferring binaries subsequently switch to evolution on much longer GW

timescales. Over time, the WD expands, GW timescales become longer, and the MT rate continually decreases. The present-day WD-NS binaries are, therefore, transferring mass at much lower rates of below $10^{-9} M_{\odot}/\text{yr}$ compared to the initial rates, e.g. Heinke et al. (2013). Even for the stably transferring systems, having a correct model of mass and angular momentum loss is important as it affects the evolution timescales and, therefore, age and population estimates.

The phase of highly super-Eddington MT lasted for about 1000 yr (Bobrick et al., 2017) (Paper I), or less than $10^{-3} - 10^{-5}$ fraction of the age of the currently observed stably-transferring systems. Nevertheless, this short phase has a deciding effect on the stability of these binaries. In the context of modelling other general stellar populations, an important conclusion is that one has to examine the evolution tracks for peculiar phases, even if such phases may appear short.

Ritter’s Equation 3 postulates that \dot{M} would vary by almost an order of magnitude if the Roche lobe radius changed by about one scale height. On an eccentric orbit, the donor star changes its relative separation to the donor by about $2ae$ over the orbit. Therefore, one may estimate that once the eccentricity e becomes comparable to $e_{\text{crit}} = h_P/R$, mass transfer from the donor will become pulsed, turning on near the pericenter and turning off near the apocenter. Importantly, e_{crit} for WD donors is very small and is typically between 10^{-4} for He WDs and 10^{-6} for very massive ONe WDs. Similar effects are also likely relevant to RG and AGB stars. Post RG or AGB-mass transfer binaries show a strong period-eccentricity ($P - e$) correlation, e.g. Vos et al. (2015, 2017), wherein eccentricities above 0.1 are common. In comparison, RG or AGB scale heights are comparable to 0.05–0.1, and therefore, MT, before the system got detached, was likely pulsed. Additionally, eccentric MT commonly occurs in triples, where the triple companion, through Kozai-Lidov interactions, makes the inner binary transfer mass on eccentric orbits (Toonen et al., 2020).

In Bobrick et al. (2017) (Paper I), we have verified numerically that one may indeed use Ritter’s formula, instantaneously applying it throughout the orbit, at least so long as the eccentricities are comparable to e_{crit} by order of magnitude. The effect of eccentricity on the J_z loss turned out negligible because the material in the disc ‘forgets’ about its initial conditions by the time of ejection. The eccentricity simulations previously performed by Regös et al. (2005) showed that at high eccentricities $e > 0.5$, the donor also loses mass through the L_3 point behind the donor, which may be significant for evolution. Early modelling by Lajoie & Sills (2011) predicted that MT is happening near the pericenter. We also pointed out that the amount of mass lost over the eccentric orbit cannot be approximated

by a delta-function, as was done in earlier secular modelling by Sepinsky et al. (2007b); Davis et al. (2013); Dosopoulou & Kalogera (2016). The reason for it is that \dot{M} rises to the peak at pericenter gradually, as a Gaussian in the Ritter case, which leads to additional eccentricity-dependent factors not included in the delta-function. Recently, this dependency was accounted for by Hamers & Dosopoulou (2019), which helped resolve issues arising at modelling low eccentricities.

The long-term evolution of eccentric binaries is complicated because eccentricity induces dynamical tides, which leads to dynamical heating of the donor (Fuller & Lai, 2012, 2013), affecting its scale height and having non-trivial effects on mass loss. Secular models with simplified assumptions about mass transfer and mass loss (compared to standard binary evolution) have been constructed in several studies, e.g. Sepinsky et al. (2007b); Davis et al. (2013); Dosopoulou & Kalogera (2016); Hamers & Dosopoulou (2019), with the most recent work by Hamers et al. (2021) also accounting for the presence of a third companion and constructing a coupling to a detailed stellar evolution code. At high eccentricities of about 0.5, one may further expect corrections to Roche lobe formalism because the assumptions of circularity and spin synchronism break down (Sepinsky et al., 2007a). These effects have so far been unexplored in secular binary evolution.

One cannot accrete much mass very quickly in a binary, and similarly, one may expect the accretion onto single remnants of mergers to be lossy in some cases. Typically, mergers of binaries, e.g. DNS (Rosswog et al., 1999), or WD-NS, e.g. Zenati et al. (2020), Bobrick et al. (2021b) (Paper III), or DWD, e.g. Dan et al. (2014), produce a central object surrounded by a dense disc. The latter, in the WD remnant case, evolves on timescales of hours due to viscosity. The accretion of the whole remnant onto the central object would require average accretion rates of about $10^2 M_{\odot}/\text{yr}$. In comparison, accretion of only a few $0.01 M_{\odot}$ onto an NS is enough to unbind the rest of the WD material. In the context of WD-NS and DNS mergers, similar questions matter significantly for whether the NS will eventually turn into a black hole, e.g. Shibata & Hotokezaka (2019). The detailed modelling of such regimes of accretion for WD-NS binaries is a matter of future studies.

The accretion onto the remnant NS is also very important for observations. The amount of mass ejected from the merger site determines how much polluting material will be delivered to the Galaxy. The amount of ejected ^{56}Ni determines the type of transient that will be observed, e.g. Arnett (1982). Likewise, the speed of the material will also be important for the duration of the transient. Finally, the total mass and the ejected composition will determine the lightcurve shape

and spectra. As we show in Bobrick et al. (2021b) (Paper III), the uncertainty in our understanding of the evolution of WD-NS merger remnants dominates the uncertainty in our understanding of the transients they produce.

More exotic physics, such as nuclear burning, may become important in some situations. In disrupting WD-NS binaries, for example, nuclear burning is expected to occur in the disc, e.g. Metzger (2012). The temperatures in the WD-NS discs can generally reach up to 10^8 – 10^9 K. The systems may reach the nuclear burning conditions in the disc given that high densities have been reached, which can only occur during mergers (Bobrick et al., 2017) (Paper I), (Bobrick et al., 2021b) (Paper III). While nuclear burning was initially thought to play a role in the dynamics of such discs (Metzger, 2012), it was later shown with more detailed 2D simulations that nuclear burning is dynamically unimportant, e.g. Zenati et al. (2019).

Consider a disc from a disrupted CO WD. Nucleosynthesis will initially proceed through the following nuclear reactions:



The burning products will further fuse with C and O, producing elements along the α -chain. Higher-order elements require higher temperatures and densities to fuse due to their larger Coulomb barriers. Therefore, in the inner regions of the disc, the highest-order elements are produced. The α -chain runs up to ^{56}Ni . However, at yet higher temperatures of about $5 \cdot 10^9$ K, nuclei photo-disintegrate, producing some amount of ^4He , and at yet higher temperatures – ^1H . The presence of H and He in the vicinity of ^{56}Ni produces iron-peak elements, such as ^{55}Mn or ^{53}Mn , potentially interesting for Galactic chemistry.

Nuclear burning in WD-NS disruptions becomes more pronounced with higher-mass WDs. This trend may be related to their larger masses, and hence densities, or perhaps to higher merger energies because of more compact orbits. The timescales for nuclear reactions are also a sensitive function of temperature. This sensitivity makes the equations of nuclear evolution stiff. In particular, the regime in which photo-disintegration into ^4He is possible has such short timescales for the α -chain reactions that the material is said to be in nuclear statistical equilibrium (NSE) (Timmes, 1999; Timmes et al., 2000). Modelling material in such a state

becomes easier because one does not need to solve for the nuclear reaction rates and can directly calculate the equilibrium compositions. However, if one does not use this simplification, the computation of such equilibrium is computationally extremely costly. In our recent study, Bobrick et al. (2021b) (Paper III), we were the first to apply an efficient public nuclear code optimized to model such conditions, and this way simulate the nuclear synthesis in WD-NS mergers with a massive WD.

1.4 Transients

Once the material gets ejected from a merged WD-NS binary, it quickly becomes gravitationally unbound. It means that the material will continue to expand homologously with a constant velocity, making the modelling relatively simple. Initially, the material is hot, about 10^8 K. However, it does not produce significant luminosity yet due to being small in size (smaller than typical stars). Due to adiabatic expansion, the material quickly cools down. Indeed, for adiabatic expansion of a monoatomic gas, the temperature depends on the density as $T \propto \rho^{2/3}$. And since $\rho \propto 1/r^3$, we conclude that $T/T_{\text{init}} = (R_{\text{init}}/R)^2$. And since the luminosity may be estimated as $L \propto R^2 T^4$, we conclude that $L/L_{\text{init}} = (R_{\text{init}}/R)^6$. Therefore, initial heat does not lead to any interesting or observable luminosity. However, the presence of ^{56}Ni heats up the ejecta when it has expanded, which makes it glow and be observed as a transient. ^{56}Ni decays into ^{56}Co with a half-life of about 6.1 d through β -plus decay, and the latter decays into ^{56}Fe through β -plus decay with a half-life of about 80 days. The gamma-rays and the positrons (β^+) particles then scatter off or annihilate with the electrons in the surrounding ejecta material, thus depositing heat. It is the radiation caused by this heat that we observe in nuclear supernovae, also from DWD mergers.

One may formulate a model for such lightcurves (Arnett, 1982) by approximately considering that all the ejecta acquired constant and comparable velocity v , which will be observed as the photospheric velocity of the transient. Then, the subsequent evolution of the internal energy U of the material with time t is described by:

$$\frac{\partial U}{\partial t} = H - L - P \frac{\partial V}{\partial t}, \quad (27)$$

where H is the heat deposited in the material per unit time, L is the energy loss due to luminosity and $P(\partial V/\partial t)$ corresponds to adiabatic cooling. Supernova fireballs are dominated by radiative pressure (Arnett, 1982). Therefore, one may write $P = U/3V$. Furthermore, since the expansion is homologous, $V \propto t^3$, and

hence $P(\partial V/\partial t) = U/3V(\partial V/\partial t) = U/t$. Therefore, Equation 27 becomes:

$$\frac{1}{t} \frac{\partial(Ut)}{\partial t} = H - L \quad (28)$$

Furthermore, the luminosity may be expressed through the internal energy by remembering that, for radiation-dominated gas, $U = \sigma T^4 V$, and that for spherical shells:

$$\frac{L}{4\pi r^2} = -\frac{4\sigma c T^3}{3 \kappa \rho} \frac{dT}{dr} \approx \frac{4\sigma c T^3}{3 \kappa \rho} \frac{T}{r}, \quad (29)$$

where κ is the opacity, while σ is the Stefan-Boltzmann constant. Therefore, we arrive at:

$$\frac{L}{4\pi r^2} = \frac{c}{3} \frac{1}{\kappa \rho} \frac{U}{Vr} = \frac{c}{3} \frac{1}{\kappa} \frac{U}{M_{\text{ej}} r} \quad (30)$$

By substituting $r = vt$, the equation reduces to $L = Ut/t_d^2$, wherein t_d is the so-called diffusion time:

$$t_d = \sqrt{\frac{3\kappa M_{\text{ej}}}{4\pi v c}} \quad (31)$$

Therefore, the full equation for the lightcurve is given by:

$$\frac{\partial L}{\partial t} + \frac{tL}{t_d^2} = \frac{t}{t_d^2} H(t) \quad (32)$$

The equation may then be integrated by multiplying both parts by $\exp(t^2/2t_d^2)$:

$$\frac{\partial(L \exp(t^2/2t_d^2))}{\partial t} = \frac{t}{t_d^2} \exp(t^2/2t_d^2) H(t) \quad (33)$$

And therefore, the solution for a bolometric lightcurve in the explicit form is given by:

$$L(t) = \frac{\exp(-t^2/2t_d^2)}{t_d^2} \int_0^t \frac{1}{t_d^2} \exp(u^2/2t_d^2) u H(u) du \quad (34)$$

Substituting the equation for ^{56}Ni decay, one can obtain the full light curves.

One would not need to assume the same temperature and luminosity for all the ejecta in the more detailed models. Normally, one would split the ejecta into velocity bins and consider the temperature, density and opacity profile of the ejecta as a function of velocity and time. In yet more detailed treatments, one would consider the propagation of shocks due to interaction with the circumstellar medium.

The above approximations are not valid in the nebular phase when the material becomes optically thin. Furthermore, replacing grey opacities with detailed spectral modelling may also affect the lightcurves, especially in particular bands. Finally, the non-LTE effects may be important if one were concerned with the detailed modelling of spectra.

2 Modelling stellar interactions

In this section, we discuss the numerical methods and techniques used for modelling stellar interactions.

2.1 3D and 2D codes for stellar interactions

We start by focussing on the interactions happening on a dynamical timescale. Interacting stars are 3-dimensional hydrodynamic objects, evolving in time, experiencing shocks, radiating energy, potentially neutrinos and undergoing nuclear burning. In the simplest case, the problem may be considered purely hydrodynamic, thus governed by the relatively simple Euler equations, e.g. Landau & Lifshitz (1987):

$$\frac{D\mathbf{v}}{Dt} = -\frac{\nabla P}{\rho} + \mathbf{f}_g, \quad (35)$$

where \mathbf{v} is the velocity of the fluid, $D/Dt \equiv \partial/\partial t + \mathbf{v} \cdot \nabla$ is the Lagrangian derivative, P is the fluid pressure and \mathbf{f}_g are the external, e.g. gravitational, accelerations. The equation expresses Newton's second law for an infinitesimal fluid parcel. The term \mathbf{f}_g may also be used to model centrifugal accelerations and Coriolis forces if one were to switch to a rotating non-inertial frame as we do in Bobrick et al. (2017) (Paper I). In addition to Equation 35, one also needs to evolve the density to ensure the conservation of mass everywhere in the fluid:

$$\frac{\partial \rho}{\partial t} + \nabla \cdot (\rho \mathbf{v}) = 0 \quad (36)$$

The above equation is called the continuity equation. Finally, one needs to model how the internal energy evolves in the fluid, which is expressed in the simplest form through:

$$\frac{Ds}{Dt} = 0 \quad (37)$$

where s is the mass-specific entropy. The fluid may be then evolved, given an equation of state (EOS) that couples the pressure P , density ρ , composition, and the thermodynamic variable, e.g. specific entropy s . Discontinuities occurring in the flow, especially for supersonic motions, are called shocks. The main effect of shocks is to average out the momentum on both sides of the shock front by turning kinetic energy into heat. Such shocks also need to be accounted for when modelling an astrophysical fluid.

The smoothed particle hydrodynamics method (SPH) represents fluids as collections of parcels of material called SPH particles. SPH particles carry physical properties such as their mass, which is constant with time, size, also called smoothing length, density, internal energy and composition. Due to such a construction, SPH method automatically satisfies the continuity equations. Also, momentum and angular momentum conservation is satisfied, up to the accuracy of the gravity solver. In the early formulations of SPH (Lucy, 1977; Gingold & Monaghan, 1977), the particle sizes were either kept constant or set to enclose the desired number of nearby particles (neighbours). The particle's properties are integrated so as to satisfy Euler's Equations 35, as described above. The equation of state, for example, could be chosen to correspond to an ideal gas, through an analytic relation, or to more complex states, such as mixtures of the partly-degenerate electron gas, ideal gas and radiative pressure, as tabulated, for example, in the Helmholtz EOS (Timmes & Swesty, 2000). The gravitational interaction may be implemented by constructing a hierarchical tree of particles (Benz et al., 1990), which allows one to quickly access the properties of groups of nearby particles (including their mass and quadrupole moment). SPH particles are integrated with individual time steps for efficient performance. The SPH particles may also experience shock interactions facilitated by artificial viscosity, e.g. Monaghan (1992). Artificial viscosity is designed to capture velocity discontinuities in the fluid. However, identifying discontinuities in discretised fluids is challenging since there is no unique way of defining them.

In our Bobrick et al. (2017) (Paper I) study, we made use of an SPH code called Oil-on-Water. Its base component, the Water code, was designed to account for the most recent developments in the SPH method at the time. One such development was implementing the formulation of SPH derived from a Lagrangian (Springel & Hernquist, 2002). In the standard formulation, the forces acting on SPH particles are obtained by discretizing Euler's Equations 35. However, this led to inaccurate forces, in particular, because the SPH particles could change their size during timesteps, in an unaccounted way. SPH formulation derived from a Lagrangian was constructed by setting up a continuous analytic relation between the particle density and smoothing length. As a result, it was possible to formulate forces that conserve energy by construction, only limited by the accuracy of the integrator and gravity solver.

We further used the Lagrangian formulation to establish an analytic upper limit on particle sizes. As a result, particles falling onto a donor or companion could interact with a limited number of particles. We also implemented an effi-

cient treatment for the fallback problem by creating dedicated arrays for handling particles with ‘too many’ neighbouring particles. It was also shown by Springel (2005) that the typically used leapfrog integration method leads to bad conservation properties for binary orbits, which is resolved, for example, by a Kick-drift-kick scheme, which we implemented. Furthermore, standard SPH implementations suffered from issues related to pairing instability, wherein particles would spontaneously clump. The issue was overcome with the introduction of Wendland kernels by Dehnen & Aly (2012). There were also developments related to the triggering of the shocks. In particular, it was recently proposed to activate artificial viscosity by using more sensitive indicators of shocks. In particular, the scheme by Cullen & Dehnen (2010) that we adopted was constructed to not trigger any artificial viscosity even in sound waves. Additionally, Saitoh & Makino (2009) improved the shock treatment by aligning the timesteps of neighbouring particles near shocks. We also introduced artificial conductivity – the method to avoid discontinuities in internal energy, e.g. Price (2012), and have updated it to also trigger only near shocks.

It was further recently found that one may formulate SPH by using different pairs of variables, such as pressure-density, or density-entropy, and others, providing better conservation properties for the variables of choice (Hopkins, 2013). Recently, new accurate integral-based estimations of gradients have been proposed (Cabezón et al., 2017), which we plan to implement in the Water code. Furthermore, in the recent paper, Rosswog (2020) proposed a new method for further improving the viscosity calculation in SPH, effectively resolving Kelvin-Helmholtz instability, which we also plan to implement.

SPH method belongs to a class of Lagrangian codes where elements follow the bits of fluid. In another Eulerian class, to which the FLASH code belongs (Fryxell et al., 2000), the fluid elements are traced at fixed locations in space. In this case, it is possible to set up structured grids, for example, Cartesian, Cylindrical, Spherical, or, generally, custom curvilinear grids. Using structured grids has the advantage that it is possible to estimate derivatives to a higher order of accuracy in grid spacing, thanks to obtaining higher-order derivatives. Similarly, equations are more easily discretized, and hence more diverse physics is generally included. A disadvantage in using Eulerian codes is that the grid has to cover the whole space, while in binary mass transfer, only a fraction of the whole volume is used. A common mitigating technique is to use adaptive mesh refinement (AMR) to add grid resolution in the required areas. The cost of using AMR methods is that changing the mesh order and re-meshing cells induces errors.

Another important issue with mesh codes is that they suffer from advection errors. In other words, a static object moving on a grid experiences spurious forces. More generally, angular momentum and mass are not generally conserved in mesh codes. Finally, Eulerian and Lagrangian codes differ in how easy it is to track the properties of systems. In summary, Eulerian codes have their unique strengths, such as the capacity for more accurate physics, and their weaknesses related to conservation and computational costs. Both Lagrangian and Eulerian codes may be used in 2D, with better performance, which is why in our studies of CO WD-NS (Zenati et al., 2020) and ONe WD-NS/BH Bobrick et al. (2021b) (Paper III) mergers, we used a 2D setup for the FLASH code.

A recent class of hydrodynamics codes is based on the moving mesh approach. For example, in the moving mesh, now public, AREPO code (Springel, 2010), the fluid is represented by a Voronoi mesh. It is an unstructured mesh, moving along with the fluid and providing a more accurate solver for the derivatives. Similarly, a more recent GIZMO code (Hopkins, 2015) uses a hybrid method of interpolating between fluid elements, with elements from SPH smoothing and unstructured grids. Even more recently, a new hybrid code has been proposed by Rosswog & Diener (2020), wherein a Lagrangian SPH code for fluid dynamics was combined with a background Eulerian grid code for modelling the general-relativistic space-time background.

Even at the highly super-Eddington phase, that determines the stability in WD-NS binaries, at $10^{-3} M_{\odot}/\text{yr}$, the amount of mass transferred per orbit, assuming a $0.6 M_{\odot}$ He WD, is only $3 \cdot 10^{-9} M_{\text{WD}}$. Since SPH codes require using comparable masses for fluid elements, modelling such a phase would require using of order 10^9 particles, which is very expensive computationally. The idea for the Oil-on-Water code, introduced in Church et al. (2009) and developed to modern form in Bobrick et al. (2017) (Paper I), is to use two types of SPH particles of very different masses: ‘Water’ particles for the stellar body and much lighter ‘Oil’ particles for the atmosphere. These two types of particles then may be kept separated on the surface of the donor star by artificial forces. This way, one can also put a significant amount of particle resolution into the transferred material, as shown in Figure 5. For example, in Bobrick et al. (2017) (Paper I), about 100K out of 400K particles were transferred from the donor, while the donor remained intact. In comparison, removing a quarter of particles from a standard SPH star would make it significantly distorted, likely leading to a dynamical merger.

In the most recent implementation, we derived the interaction potential for the two types of particles starting from a Lagrangian, and thus avoiding dissipative

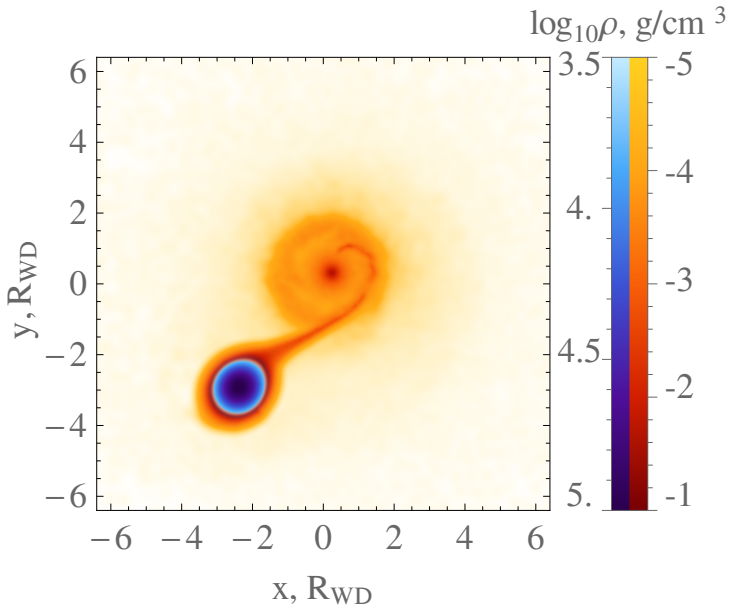


Figure 5: A density snapshot in the horizontal plane from our simulation of a WD-NS binary with a $0.15 M_{\odot}$ WD and a $1.4 M_{\odot}$ NS with the Oil-on-Water code, from Bobrick et al. (2017) (Paper I). The code splits the material in the donor WD into two types of particles corresponding to the stellar body (Water) and the atmosphere (Oil). Such a distinction allows one to put significantly more mass resolution into the particles participating in mass transfer than other methods.

forces acting on Oil particles. We also optimised the gravitational tree by noticing that lightweight particles are not affected by their self-gravity. Since gravity is typically the most computationally demanding part of hydrodynamic codes, the code efficiency improved by a factor of several.

Implementing realistic scale heights $h_P \approx 10^{-5} R_{\text{WD}}$, as in the WD donor case, is not possible since the size of SPH particles cannot be much larger than the scale height. However, it is possible to adjust the boundary between the two types of particles to obtain a desired mass transfer rate. Since the outer zone of the donor is now well resolved, and since the scale height was set to be about $h_P/R_{\text{WD}} \approx 0.024$ in the standard setup, the critical eccentricity for pulsed MT becomes $e_{\text{crit}} \approx 0.024$.

Due to such low critical eccentricity, the binary setup becomes sensitive to the few per cent corrections to the orbit. This sensitivity, in particular, made us develop a new relaxation scheme, wherein the donor WD is relaxed on a corotating orbit, under viscous forces, with the separation gradually decreasing until after the start of MT. The binary then is initiated with the MT stream already open, close to the steady mass transferring state. The code was sufficiently sensitive, for example, to detect the dependency of the orbital frequency on quadrupolar interactions, which affect the Kepler's law, $v_{\text{orb}}^2 \propto M_{\text{NS}}M_{\text{WD}}/a$, by several per cent, and the dependency of the donor volumetric radius on binary separation, which may be between a few per cent and up to 15 per cent for nearly equal-mass binaries. These corrections to the orbit also explained the oscillations in MT rate seen in earlier works simulating mergers of DWD binaries, e.g. Dan et al. (2011).

2.2 1D stellar interaction codes and population synthesis

Currently, 3D codes provide the most accurate and detailed method for theoretically investigating astrophysical processes. Such codes may help one choose among the most likely scenarios, bring intuition, or model complex processes that are not accessible otherwise. Ultimately, all the astrophysical models should probably have an understanding based on 3D codes.

One fundamental limitation for 3D codes is the development cost since there is no general-purpose code that can allow one to simulate any astrophysical problem. Another fundamental limitation is the computational cost, which means that only a few physical situations may be analysed, implying a longer development cycle. A good rule of thumb is that 3D codes are best at assessing dynamical timescales for systems, which means that longer timescales, e.g. thermal, or MT timescales are not accessible. Finally, even in 3D studies, it takes more than one

study to converge on the relevant physics fully.

In binary mass transfer, interactions may take a long time. The longer-term interactions are best captured by 1D codes, such as MESA (Paxton et al., 2011). The 3D codes then may be used to calibrate the models of 1D codes. For example, as discussed earlier, in the binary evolution code MESA, mass loss is parameterised by the amount of mass lost by the binary and by the angular momentum carried away from the binary. Such parameters are a function of mass transfer rate and likely, other parameters, for example, accretor mass (which may affect the accretion efficiency) or metallicity (which may affect magnetism and wind processes in mass ejection). These parameters should be in agreement with the results from 3D codes. For example, in WD-NS inspirals, the phase of intense MT has the strongest effect on stability. The Oil-on-Water model was applied to this regime to produce the parameters for this important phase. We ensured, in particular, that the parameters in the 3D simulation are not varying with time, i.e. the simulations have entered a quasi-steady regime. Generally, one would need to make a dedicated simulation for every relevant MT rate \dot{M} . In the modelling of WD-NS binaries, however, this process was simplified by the fact that the SPH equations are invariant to the Oil particle mass. Therefore the reconstructed parameters apply for any mass transfer rate (at which the physical assumptions, e.g. of a non-accreting NS, hold).

To simulate the lives of stars on thermal or nuclear timescales on present-day computers, one may use 1D stellar evolution codes like MESA (Paxton et al., 2011) or Eggleton’s code (Eggleton, 1971, 1972). In these cases, stars are split into concentric spherical shells, with their properties evolved in time. Thanks to a lower number of spatial dimensions, it is possible to evolve the stars for a much longer time. The accuracy of such solvers is high enough, for example, to explain solar pulsations with errors smaller than 10^{-3} (Paxton et al., 2013). The 1D setup also makes it easier to implement and test physics components. The modern version of MESA includes detailed radiative and neutrino transport, hydrodynamics, white dwarf crystallisation, element diffusion, stellar oscillations and other prescriptions (Paxton et al., 2018, 2019). Intrinsically 3D effects, such as convection or stellar spin, have also been implemented in MESA, in the averaged sense, as effective prescriptions. 1D codes are currently the only way to evolve stars through all phases of their evolution, taking between hours to days to compute on a single core.

Furthermore, 1D codes have been successfully applied to model binary evolution, e.g. Paxton et al. (2015). In the current implementation, the code evolves the

detailed structure of both stars, along with several parameters related to the binary evolution, such as the semimajor axis, eccentricity and the mass transfer rate. Since binary interactions are intrinsically a 3D phenomenon, 1D codes strongly rely on the models of binary evolution, such as mass transfer efficiency, angular momentum loss, eccentric mass transfer and common envelope prescriptions, supplied by detailed 2D and 3D models. With these caveats in mind, binary MESA code is currently the most accurate method of modelling long-term stellar evolution.

Since a single binary in MESA may be evolved over about 10 hours on a single core, stellar evolution codes like MESA can be used to model binary populations. Several such studies have been performed, e.g. Vos et al. (2020) (Paper II), Van et al. (2019); Laplace et al. (2020); Klencki et al. (2021) among others. Due to computing limitations, all such studies have been performed with populations of up to a few 100K binaries. This number limits the applicability of such population modelling to relatively common outcomes of binary evolution and allows one to explore relatively few parameters. Another complication is that traditional binary evolution prescriptions, such as common envelope evolution, and evolving the outcomes of common envelope evolution, requires an additional external interface. Further yet, currently, there are only a few software tools for treating populations of MESA-simulated binaries and especially handling the exceptions. These require both an efficient interface for investigating individual binaries and an additional tool for treating populations. In summary, population synthesis with detailed structure codes is best suited for modelling relatively expected outcomes of initial populations and for exploring only a small number of free parameters.

Population synthesis approach models stars or binaries, effectively in zero dimensions, evolving a small number of parameters describing the star and the binary. Population synthesis models for single stars have been calibrated by the more detailed 1D codes, as has been done, for example, in the classic SSE code (Hurley et al., 2000). However, more subtle details of single evolution, such as the conditions for non-degenerate helium flash, are still lacking to a large extent in population synthesis codes. For this reason, several hybrid methods coupling MESA and population synthesis codes have emerged, suitable, for example, for treating the CE phase (Kuranov et al., 2020; Bavera et al., 2021). Similarly, just like with MESA, binary population synthesis codes have to be calibrated by the detailed models of binary evolution. By reducing another dimension, population synthesis codes can be used to model populations of billions of binaries at the cost of accuracy. The computational capacity allows one to systematically explore the impact of large numbers of parameters, e.g. Broekgaarden et al. (2019). One ben-

enefit of doing so is that the uncertainties in binary evolution may be parametrized, and the parameters may be optimized to match observations. In the long term, ideally, the population synthesis codes will be able to explain all the observations and have all their parameters calibrated by 1D and 3D codes.

Stars, and especially massive stars, are born in clusters, e.g. Oh & Kroupa (2016). The cluster environment leads to dynamical interactions, in particular perturbing the orbits of binary stars and producing stellar mergers. During such interactions, the evolutionary histories of single and binary stars are affected. In this sense, there is no truly isolated binary evolution, e.g. Banerjee (2018). In dense environments, such as the cores of globular clusters, such perturbations may be a dominant process in binary evolution, e.g. Davies (1995). Compared to simulating binary populations, where binaries evolve independently, cluster populations, as, e.g. in Bobrick et al. (2021a) (Paper IV), have to be evolved together. In this case, during the binary evolution timesteps, the cluster environment code has to evolve the variables related to the cluster. Additionally, the dynamical interactions between the single and binary stars have to be modelled either through analytic methods, e.g. Ginat & Perets (2020); Stone & Leigh (2019) or numerical models, e.g. Fregeau & Rasio (2007). In the simplest implementation, e.g. Ivanova et al. (2006, 2008), Bobrick et al. (2021a) (Paper IV) the cluster may be modelled in zero dimensions, being described by core, halo and several other parameters. In more detailed implementations, e.g. Giersz (2001); Fregeau & Rasio (2007); Askar et al. (2017), the cluster model is evolved in 1D along with the stars. In yet more detailed and computationally expensive setups, the clusters are modelled in full detail as self-gravitating N-body systems (Wang et al., 2016).

When considering the modelling of clusters, the hierarchy of codes is similar to that of stellar evolution. The coarsest approximations to the cluster evolution serve as rapid exploratory codes that may help fit the models to observations. The more detailed 1D cluster codes are currently the most accurate and affordable way of approximating populations of up to 10K clusters. Such a number is sufficient to model the MW cluster system 100 times. Finally, the most accurate cluster codes based on NBody modelling allow one to model only several clusters to calibrate the faster models.

In order to model the outcomes from cluster populations, the clusters must be initialised in their environment. In our Bobrick et al. (2021a) (Paper IV) study, for example, we consider all the star clusters in the Galaxy. Modelling the full Galactic population of stellar or globular clusters is necessary for predicting the observations of sources from the cluster environment. In this sense, cluster populations gener-

ally also have to be studied in groups representing their host environments. In the context of binary evolution, host-based populations have been implemented, for example, in the BPASS code (Eldridge et al., 2017), wherein the populations are used to obtain the combined spectra from the hosts, for example galaxies.

2.3 Other specialised codes

In cluster environments, stars and binaries interact dynamically with each other. For example, in the core of 47 Tuc cluster, a typical binary of solar-like stars experiences one encounter within a few $10 R_{\odot}$ within 1 Gyr, e.g. Davies (2013). Similarly, about ten per cent of massive O and B stars are runaways, e.g. (Gvaramadze et al., 2012). This implies that at least 10 per cent of O and B stars experience strong interactions, and yet more experience weaker interactions. During close encounters between a binary and a single star or a binary and a binary star, the stars tend to undergo chaotic 3- or 4-body interactions. In this case, the evolution of stars is impossible to model analytically (only statistically). After the interactions, the least massive stars tend to be ejected, and the binary may well exchange components, or stars may experience mergers.

The Fewbody code is a compact N-body integrator aimed at modelling systems with a small number of objects (Fregeau & Rasio, 2007). In the default setting, the code uses direct integration methods, i.e. without regularisation schemes, and dynamically identifies the formation of hierarchical systems. Stellar mergers, for example, are identified based on the sticky-sphere approximation, i.e. when two stars pass within a certain distance from each other. The code, in particular, can then report the final products of interactions (single, binary, triple stars and mergers) and their orbital properties. For the cluster simulations, then, the NBody code is called when a pair of stars or binaries are identified to have experienced an encounter. Subsequently, the parameters of stars are used as inputs for further binary or Galactic orbital evolution, as is the case with the Bobrick et al. (2021a) (Paper IV) study.

Other examples of specialised codes are nuclear evolution codes. These codes predict how nuclear composition and thermodynamic properties of material change with time as a function of initial compositions, density, temperature and electron fraction. Nuclear evolution equations are non-linear because the nuclear reaction rates may be proportional to the abundance of a single element $\mathcal{R} \propto Y_i$, as in the case of nuclear decay, pairs of elements $\mathcal{R} \propto Y_i Y_j$, as in the case of nuclear fusion, and to third powers of element abundances $\mathcal{R} \propto Y_i Y_j Y_k$, as, e.g. is the case for the triple-alpha reaction. Nuclear evolution equations are also stiff, as in specific

regimes, e.g. at high temperatures, the reaction rates may become extremely large compared to other regimes, e.g. at lower temperatures.

For these reasons, nuclear networks are mathematically hard to implement. When it comes to nuclear post-processing, additional complexity is that depending on the elements one is interested in, one has to simulate large numbers of isotopes, of order 100. In the simplest implementations, nuclear networks are based on direct integration of nuclear equations with a stiff solver and an α -element network, using between 7 and 21 elements. Such networks, for example, are used as a basis of the FLASH (Fryxell et al., 2000) nuclear solver. More complex networks, such as MESA PPN (Paxton et al., 2011) are based on more detailed networks of more than 100 elements, while yet more detailed networks, e.g. Torch (Timmes, 1999; Timmes et al., 2000), additionally implement optimised algorithms to model nuclear evolution. For example, the capability of the Torch code to model nuclear statistical equilibrium has been necessary for modelling the mergers of ONe WD-NS binaries in our Bobrick et al. (2021b) (Paper III) study. It is important to be aware that experimental nuclear data may limit the accuracy of nuclear networks. For example, as shown by Costa et al. (2021), uncertainties in the experimental data may affect astrophysical predictions, for example of the late evolution of massive stars.

Nuclear codes are used for post-processing when the feedback from nuclear reactions is dynamically and thermodynamically unimportant. This is the case for WD-NS mergers, e.g. Zenati et al. (2019). In this case, nuclear networks are applied to evolutionary trajectories from hydrodynamic simulation. Lagrangian codes, such as the SPH Water code, are particularly well suited for nuclear post-processing since the method directly allows one to extract particle evolutionary trajectories. In Eulerian codes for example FLASH, in comparison, the post-processing has to be applied to tracer particles, which are fictitious particles that follow the motion of fluids. In more detailed FLASH implementations, the hydrodynamic runs are executed together with an alpha-network on the fly, with the post-processing applied on top. In all cases, nuclear evolution for each fluid element significantly extends the number of particle properties that one needs to simulate, compared to direct hydrodynamic simulations.

Another example of specialised astrophysics codes that we used is the SuperNu code for supernova spectral synthesis (Wollaeger et al., 2013; Wollaeger & van Rossum, 2014). The SuperNu code constructs detailed lightcurves and spectra for homologously expanding ejecta, including relativistic corrections. The code solves radiative transfer equations in 3D, 2D, 1D or spherical 1D geometries.

The radiative transfer equations are essentially solved by considering material in different velocity bins and groups of radiation particles in different frequency bins propagating on the background of the velocity bins. Since the photon diffusion timescale may be much shorter than the timescale of the transient, the particles are generated continuously through the simulation. SuperNu is one of the few codes capable of synthesising supernova spectra, along with CMFGen (Hillier & Lanz, 2001), Sedona (Kasen et al., 2006) and Stella (Blinnikov & Bartunov, 1993; Moriya et al., 2011) codes. Compared to other codes, it is open source and has the most optimised methods for simulating radiative transfer, although in local thermodynamic equilibrium (LTE) approximation.

In our Bobrick et al. (2021b) (Paper III) study, we used a relatively standard method of initialising SuperNu simulations. The code was initialised by setting up a grid of velocity bins, which were assigned densities, temperatures, initial time, electron fractions, compositions and ^{56}Ni , ^{56}Co abundances of the ejected material. The code assumes homologous expansion, or in other words that the material expands at constant velocities. At different moments in time, the code outputs spectral energy distributions (SEDs) and overall parameters of the ejecta. In our study, these SEDs were convolved with the transmission curves for filters used in transient observatories, thus producing lightcurves.

Future radiative transfer codes will likely be including non-LTE effects as is done, e.g., in the STELLA code, but have optimisations similar to those implemented in SuperNu. Another important avenue is constructing a radiative transfer code that includes the effects of energy injection from fallback accretion, e.g. Dexter & Kasen (2013), from subsequent mass ejection or circumstellar material (CSM) interactions, e.g. Chevalier (1982). Generally, supernova spectral synthesis codes should be used in conjunction with binary interaction codes to simulate spectral signatures of binary interactions.

3 Comparing models against observations

In this section, we discuss the various modelling aspects that arise when comparing the theoretical predictions for interacting binaries with observations.

3.1 The Galaxy: chemistry and kinematics

Let us start by considering Galactic populations of interacting binaries. The Galaxy consists of several components with different age and star formation history (Robin et al., 2003). The thin disc dominates the local stellar density and has a range of ages. The thick disc makes about 10 – 20 per cent of stellar mass in the Galaxy but is made of old stars having ages of about 10 Gyr. Therefore, in local samples of a few tens of objects or more, a few may be from the thick disc, given the object may reach old ages. Similarly, the central bulge contains a 10 Gyr old population but is usually harder to access observationally. Finally, the halo makes a tiny fraction of the total Galactic mass, of order 10^{-3} , and has a very small local density, thus showing up only in large samples of more than 1000 objects.

The different components also differ by metallicity and alpha-element abundances. For example, in the thin disc, the age is correlated with metallicity, e.g. Bensby et al. (2003). The average metallicity of old thin-disc stars is about -0.4 dex. Similarly, the thin disc shows a radial metallicity gradient of about 0.07 dex per kiloparsec (Robin et al., 2003). Similarly, the thick disc has a low metallicity of about $[\text{Fe}/\text{H}] = -0.8$, and is enhanced by alpha-elements. Metallicities and, potentially, alpha-element abundances (Fu et al., 2018) may be important for the evolution of giants, as discussed earlier. Kinematics of stars in the Galaxy is also affected by age and varies with Galactic components, with older stars being dynamically hotter. Metallicity history in the Galaxy has been modelled in great detail within Galactic studies.

Long-period sdBs are a good example of interacting binaries showing the imprints of the Galactic history (Vos et al., 2020) (Paper II). These binaries show a correlation between their periods P and their mass ratios q , which had been hard to explain purely by binary evolution models. Long-period sdBs are observed locally, within the nearby 500 pc – 1 kpc. Their periods vary from a few 100 days to a bit more than 1000 days. Their identification is made through follow-up spectral observations and complex spectral analysis. Therefore, the current sample is slightly larger than 20 objects, e.g. Vos et al. (2018). Long-period sdB stars form from progenitors of all ages, in which the primary has reached the RG stage.

As we showed in Vos et al. (2020) (Paper II), the main effect of metallicity

is to change the final period of the binary. This is related to the fact that higher metallicity makes RGs larger, at a given core mass, leading to wider orbits for RLO and wider final orbits. Accounting for the correct Galactic metallicity history from Robin et al. (2003) fully explained the correlation. It was possible to establish this connection through the use of MESA code-based population synthesis. Long-period sdB binaries are the first interacting binaries to have shown the imprints of the Galactic metallicity history.

Another population where the Galactic context is important is the runaway O and B star population, i.e. the population of O and B stars moving at a velocity higher than 30 km/s relative to the local standard of rest. Massive O-type stars, for example, form in clusters and live for only about 10 Myr. Nevertheless, about 5–10 per cent of all O and B stars are known to be runaways, and 20 per cent are found outside of their hosts. Runaway stars may travel hundreds of parsecs from their hosts. The Galactic locations of these stars, e.g. remoteness from star-forming regions or the disc plane, may help their runaway identification, e.g. Oh & Kroupa (2016).

There are two historic channels for making runaway stars. The isolated evolution channel suggests that massive runaway stars form because their companions exploded as a supernova, launching them on runaway orbits (Blaauw, 1961). However, it was recently realised that this channel only predicts that 0.1 per cent of O stars become runaways (Renzo et al., 2019). The reason is that for the supernova to lead to a high kick, the binary has to be tight. At the same time, in tight binaries, primaries get stripped by companions before they become supernovae. As a result, the kick is typically below 30 km/s. However, the isolated channel may contribute significantly to walkaway stars, i.e. slower stars unbound to any particular cluster. The other channel for producing runaways is through dynamical interactions in clusters (Poveda et al., 1967). In this scenario, massive stars sink into the cluster cores and interact with other massive stars in the cluster cores, being kicked out, typically, by binary-binary interactions (Leonard & Duncan, 1990). The channel can explain runaway O and B-type stars. Therefore, in the Galactic environment, O and B-type stars primarily trace the young component of the thin disc. Additionally, they are offset from the birthplace due to their kinematics.

O and B stars and the resulting red supergiants (RSGs) may be observed from much of the Galaxy. Similarly, RSGs can be even observed from the Large and Small Magellanic Clouds (LMC and SMC) and other galaxies. The expected observed locations of the synthetic populations may be identified by integrating the

orbits in the Galactic potential.

3.2 Using models to synthesise observations

The models of runaway RSG stars, for example, or models of sdB binaries may be connected to observations through synthetic photometry. Photometric identification may be obtained, for example, from the knowledge of effective temperature and luminosity.

In more detailed implementations, one may synthesise photometric bands. For non-interacting single stars and binaries, one may make use of pre-calculated stellar evolution tracks and isochrones. Such tracks are based on 1D stellar evolution codes, simulated for grids of stars covering a range of initial masses and metallicities. For example, in Bobrick et al. (2021a) (Paper IV) we use MIST tracks (Choi et al., 2016) based on simulations with MESA code. Recently, a method for automatically interpolating between such tracks has been introduced by Agrawal et al. (2020). Stellar evolution tracks, within MIST, provide the effective temperature and luminosity for stars, which, assuming black-body spectrum was convolved with bands for filters used in observations. The photometric magnitudes in different bands are directly tabulated in the MIST catalogue, and we use these in our study of runaway red supergiants. Similarly, we use MESA-code based photometric parameters in our study of sdB binaries in Vos et al. (2020) (Paper II). For systems emitting in other wavelengths, e.g. radio or X-rays, one would also need to reconstruct luminosities in desired bands, although with more specialised codes.

Even having obtained the expected photometric appearance of the modelled systems, one needs to account for extinction between us and the typically observed sources. For example, the sources in the Galaxy may be affected by dust extinction, dimming and reddening the optical observations. There are tabulated Galactic dust maps, e.g. Lallement et al. (2014), which allow one to correct for such effects.

In practice, modelling of the observational counterparts often does not require accounting for extinction. This simplification is possible because dust correction is typically done by observers. However, understanding the magnitude of the effects may be very important for modellers since extinction effects may introduce significant biases in observations. The biases may affect systems with different parameters (e.g. masses, ages, metallicities, luminosities) very differently, thus introducing a gap between the modelled populations and observations. Such biases may be removed by modelling the processes which introduce the biases or else by dealing with reduced observational samples wherein the biases are not present.

Even having accounted for the extinction and even possible biases, one needs to make sure that one understands how the observed objects are identified. In other words, one needs a model of how observations are made. A good example is long-period sdB binaries, as discussed in Vos et al. (2020) (Paper II). For example, even if the synthesised population predicts a binary containing an sdB star, i.e. a core- or shell-helium burning hydrogen-deficient subdwarf of spectral class B, it does not mean that it would have been observed and identified as such.

The observational sample of sdB binaries is based on follow-up observations of candidate systems. The candidate systems are identified based on photometric criteria, e.g. the ones from Geier et al. (2017), applied to *Gaia* photometric bands. The modelled systems not satisfying these criteria would not be inspected by observers. Furthermore, even assuming the observed object was selected for observations, its identification as an sdB binary is made spectroscopically by requiring that the contribution of the sdB star spectrum at the peak wavelength of its companion is not larger than 90 per cent and not less than 10 per cent and vice versa. Therefore, to ensure that Vos et al. (2020) (Paper II) modelled the actually observed systems, we synthesised the spectra from the modelled binaries and examined whether the spectra satisfy such conditions. A similarly detailed analysis is generally speaking necessary when modelling observed samples of any objects. Therefore it is very important to have homogeneous, well-understood and straightforward criteria for observational identifications.

The observational model in our study of the transients from ONe WD-NS/BH mergers in Bobrick et al. (2021b) (Paper III) is different from the one adopted to sdB-MS binaries. Since the observational counterparts are unknown, we modelled a generic process of transient detection. A transient identified by a synoptic survey will be detected if it reaches an apparent magnitude sufficient for its detection in the used bands and if it lasts during a time at least comparable to the revisit time of the same parts of the sky. For example, the Vera Rubin Observatory (LSST) will be scanning a large fraction of sky in *ugrizy* bands at least weekly, with the sensitivity down to the *r*-band magnitude of 24.7 (LSST Science Collaboration, 2009). Photometric or spectroscopic observations may then follow the transient. The photometric observations may be performed in the same or other optical or more general electromagnetic bands. Therefore, we modelled the lightcurves for the transients since the shape of the lightcurves in different bands may be used to identify the transient. Similarly, we synthesised the observed spectra so that they may be compared to spectroscopic surveys. We also considered discrete constraints, such as the presence of hydrogen lines and the properties inferred from

lightcurves or spectra, such as the photometric velocities or ^{56}Ni abundances, to help the identification.

For the ONe WD-NS/BH mergers, the gap between the models and observations is much wider than in the long-period composite sdB study. In particular, several theoretical models appear comparably plausible at the moment. The difference is related to our ignorance of the detailed evolution of the remnants from WD-NS/BH mergers. In our study, we found an observational counterpart transient, the faint end of type Iax supernovae, which may reproduce the observed properties of the transients. However, this is still a tentative identification. A confident identification, likely possible with the large observational samples provided by the Vera Rubin Observatory (our study predicts between a hundred and a thousand detections every year), will allow one to identify these transients with more confidence and, conversely, constrain the properties of the transients.

Another, perhaps simpler way of producing the observed signatures of the interacting binaries is related to the observed detection rates of the binaries and of the relevant observed systems. For example, in the study of stability of the onset of mass transfer in WD-NS binaries (Bobrick et al., 2017) (Paper I), the onset phase itself is too short to be observable. However, WD-NS binaries surviving the onset of mass transfer are expected to turn into ultracompact X-ray binaries (UCXBs), with their composition reflecting the composition of the WD.

Therefore, since the number of surviving sources strongly depends on the stability of mass transfer, the theoretical model of stability has a strong observational test. In particular, Bobrick et al. (2017) (Paper I) analysed the number of observed progenitor WD-NS binaries relative to the number of stably surviving companions. In comparison, Toonen et al. (2018) predicted the population of stably-transferring UCXBs in the Galaxy directly from population synthesis.

Finally, as another facet of the observational manifestation of interacting binaries, one may consider their indirect manifestations through other objects in astronomy. As an example, we consider the chemical enrichment of the Galaxy in ^{53}Mn by ONe WD-NS binaries in Bobrick et al. (2021b) (Paper III). The Galaxy was initially metal-poor, and the products of stellar evolution enriched it with alpha elements over time. Current models suggest that core-collapse supernovae produced most of the light elements, while type Ia supernovae produced most of the Galactic iron-peak elements, e.g. Edvardsson et al. (1993); Nomoto et al. (2013). However, for a stellar population, core-collapse supernovae occur within 10–100 Myr, while type Ia supernovae occur on timescales comparable to 1 Gyr, e.g. Maoz et al. (2012). Therefore, one can use metallicity, $[\text{Fe}/\text{H}]$, of the present-

day Galactic stars as an indicator showing at which epoch did type Ia supernovae start affecting the Galactic chemistry.

Type Ia supernovae are believed to be the main polluter of the Galaxy by ^{53}Mn (Seitenzahl et al., 2013b,a). For this reason, the present-day history of how ^{53}Mn was added to the Galaxy should be visible when analysing stars with metallicities $[\text{Fe}/\text{H}] \gtrsim -1$, which are believed to have been affected by type Ia supernovae. However, the ONe WD-NS binaries also produce ^{53}Mn , with individual explosions comparable to the yields from type Ia supernovae (Bobrick et al., 2021b) (Paper III). Given that ONe WD-NS mergers make up 6–20 per cent of type Ia supernova rate, they may account for up to 20 per cent of the present-day ^{53}Mn in the Galaxy. Moreover, if ONe WD-NS mergers occurred on timescales faster than type Ia supernovae, as allowed by the current models (Toonen et al., 2020), they could have even larger contributions in the early Universe, which may be potentially assessed through analysing low-metallicity stars.

3.3 Using observations to constrain the models

In some instances, the observations may provide more input than simulations. The observations may then be used as an important guide to confirm or discard the theoretical modelling. For example, in our study of runaway RSGs, the observational data on Betelgeuse is very constraining. Betelgeuse is observed to be rapidly spinning, both based on its HST (Uitenbroek et al., 1998) and ALMA (Kervella et al., 2018) observations. Such rotation is unusually high for the typical measurements of RSGs. Furthermore, Betelgeuse is observed to have high $[\text{N}/\text{C}]$ and $[\text{N}/\text{O}]$ abundances, also typical to rapidly-rotating stars (Lambert et al., 1984).

Similarly, observations of Betelgeuse strongly indicate that it is a runaway star (Harper et al., 2017). Additionally, observations of Betelgeuse show a bow shock produced by the collision of its wind and the interstellar medium, and the shape of the bow shock also matches its runaway origins (Mohamed et al., 2012; Decin et al., 2012). Even further, Betelgeuse is observed to have atypically strong asteroseismic oscillations (Joyce et al., 2020). Therefore, observations of Betelgeuse, for example, strongly suggest that it is an unusual red supergiant. Moreover, the diverse unusual features of Betelgeuse match well with the predictions from the scenario in which it formed from a merger on a subgiant branch, e.g. Chatzopoulos et al. (2020).

The fact that Betelgeuse might be a merger is also hinted at by observations of the progenitors – main-sequence O and B stars. Indeed, as we discussed earlier, about 20 per cent of young massive stars are observed to be away from their host

cluster environment, and about 5–10 per cent of all massive young O and B-type stars are observed to be runaway (Gvaramadze et al., 2012). Furthermore, about 70 per cent of runaway stars are found to be in binaries (Chini et al., 2012). Therefore, it is observationally expected that a fraction of runaway O-stars will have experienced binary interactions, and some fraction of them will have merged when the primary star is on the subgiant branch.

Similarly, it is believed that mergers of relatively massive B stars on the main sequence produce rapidly-spinning Be stars with a disc surrounding them (Rivinius et al., 2013). The observations of the Galactic runaway Be stars indicate that they are single and comparable in numbers to the population of runaway B stars (Boubert & Evans, 2018). This observation supports the idea that a fraction of massive runaway stars experiences a merger before the primary develops into an evolved red supergiant.

Observational data may also be used in the form of a dataset. For example, in the Bobrick et al. (2021a) (Paper IV) study, we used the public Simbad database (Wenger et al., 2000). Simbad database stores most known stellar objects and most of the existing direct measurements for such objects. For example, for RSGs, one may find their positions, distances and kinematic data, and the existing measurement of magnitudes in different bands and inferred parameters, such as their rotations, surface gravities, spectral classifications and others, if available.

One may also access the data from more uniform datasets. For example, in the the same project, Bobrick et al. (2021a) (Paper IV), we accessed *Gaia* eDR3 dataset (Gaia Collaboration, 2016; Bailer-Jones et al., 2021) to measure the positions, magnitudes and colours of the objects we identified. By assessing the *Gaia* eDR3, this way, we obtained the most recent and accurate observations of our systems. Finally, one may also directly search the literature sources as, e.g., was done by Comerón & Figueras (2020), who surveyed the literature for known runaway RSGs. When available, literature compilations may be very valuable for relatively small specialised datasets.

In the context of our study of the onset of mass transfer in WD-NS binaries, Bobrick et al. (2017) (Paper I), the observations have been providing the most direct constraints based on the rates. Indeed, WD-NS binaries before spiralling into contact may be observed as binary radio pulsars. After a WD-NS binary spirals in, it may or may not survive the onset of mass transfer. In the first case, the binary may evolve further into an ultra-compact X-ray binary, while in the other case, the binary will merge and produce a supernova-like transient. Estimating the observational formation rates for such objects may then be used to constrain the

models.

For the progenitors, the magnetic field of the spinning NS produces a periodic radio signal with may be detected by the ground radio facilities. The orbital motion of the NS in the binary leads to delays in arrival times of the periodic signal, allowing one to estimate the binary orbital period and the minimal mass of the companion. Follow-up optical observations may then help identify the companion as a white dwarf. Some such binary pulsars may be then predicted to spiral into contact due to the emission of gravitational waves. One may estimate the actual number of binary pulsars that will spiral into contact in the Galaxy by accounting for the effects of pulsar beaming, i.e. accounting for the fact that pulsar emission may be only seen from specific directions (Kalogera et al., 2001), and for the sensitivity of pulsar searches (Kim et al., 2004).

Similarly, for the outcomes, one may use the observations of the Galactic UCXBs. In this case, the period of the X-ray binary may be obtained from the periodicity in the X-ray pulsations of the system. The orbital periods may be used to estimate the ages of the systems. Furthermore, the observed X-ray luminosity may be used to estimate the mass transfer rates and hence further constrain the ages of the systems. It is generally believed that persistent UCXBs are detected from across the whole Galaxy (Heinke et al., 2013), allowing one to obtain their field formation rates. Since UCXBs may form from other channels than WD-NS binaries (van Haaften et al., 2013), the observed formation rates of UCXBs serve as an upper bound on the number of stable systems produced by inspirals of WD-NS binaries. In particular, the formation rates of UCXBs with helium composition are observed to compare reasonably well to the inspiral rates of He WD-NS binaries. In contrast, the inspiral rates of WD-NS binaries with CO or ONe WDs are more than an order of magnitude larger than the formation rates of UCXBs showing C, O or Ne composition.

The rates of observed optical transients are a weaker probe of WD-NS binary inspirals. The existing all-sky surveys, e.g. PTF (Law et al., 2009; Rau et al., 2009), Pan-STARRS (Chambers et al., 2016), ZTF (Bellm et al., 2019), ATLAS (Smith et al., 2020) are discovering thousands of optical transients every year. There are several tens of types of optical transients currently known, e.g. Milisavljevic & Margutti (2018). In our original study in Bobrick et al. (2017) (Paper I), we assumed that WD-NS binaries may produce Ca-rich gap transients, which are relatively faint peculiar transients with estimated occurrence rates close to the expected rate from WD-NS binary mergers. Since then, Frohmaier et al. (2018) revised the formation rate for Ca-rich gap transients significantly upwards, while

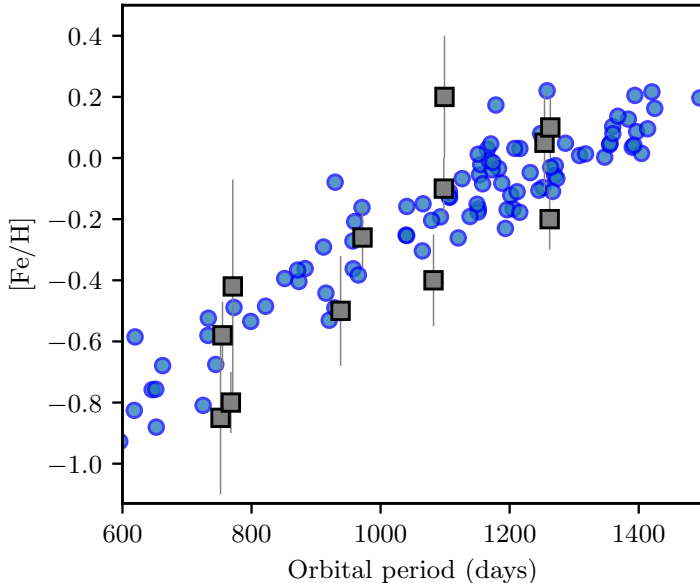


Figure 6: An image from Vos et al. (2020) (Paper II) showing the distribution of periods and metallicities in the observed and synthesised populations of sdB binaries. Since the agreement has been achieved without any explicit fine-tuning, it may serve as an indication that we probably understand the observed population of sdB stars.

further observations of these transients led to the rates being revised back down (De et al., 2020). Later, with more detailed observational predictions for WD-NS mergers in Bobrick et al. (2021b) (Paper III), it became possible to compare the models for lightcurves and spectra to the observed transients. This more detailed comparison made it possible to connect the models to the faint end of type Ia supernovae. Eventually, the detailed identification of the transient will hopefully provide further constraints on mergers of WD-NS binaries.

A good example where observations may be very constraining for the models comes from our study of long-period sdB binaries (Vos et al., 2020) (Paper II). The presently-observed long-period sdB binaries show strong evidence that the mass transfer process that led to the formation of these binaries was non-conservative (Vos et al., 2018). Indeed, long-period sdB stars form when red giants lose their envelopes, between 0.3 and $1.5 M_{\odot}$, due to interactions with their main-sequence companions. If the companions accreted an amount of material larger than about $0.01 M_{\odot}$, they would show significant rotation, which they do not show. Simi-

larly, a significant amount of accretion of the RG material onto the MS companions would lead to anomalous CNO abundances in the MS stars, which is also not observed.

However, a further constraint is possible because we likely understand the details of the formation of long-period sdB binaries. Indeed, since our MESA-based populations are consistent with the orbital properties, metallicities, as we show in Figure 6, and, generally, the observed rates of long-period sdB binaries, we have some confidence that we may be understanding the population. The observed population then rules out the possibility of conservative mass transfer in these systems. Indeed, assuming then that mass transfer onto the MS companions was conservative even beyond the accretion rates of $10^{-5} M_{\odot}/\text{yr}$ leads to the range of present-day mass ratios that strongly disagrees with the range in the observed systems. Therefore, with these things in mind, we conclude that RGs in our sample lead to non-conservative mass transfer, at least for the rates above $10^{-5} M_{\odot}/\text{yr}$ and for accretor masses of up to $1.5 M_{\odot}$.

In this case, the constraint is strongly motivated observationally. Moreover, since mass loss is mostly determined by what happens near the accretor, the constraint also applies to all other similar binary systems, not only sdB progenitors. In such binaries, an MS star of less than $1.5 M_{\odot}$ or so is undergoing disc accretion through Roche lobe overflow from a companion at mass transfer rates above $10^{-5} M_{\odot}/\text{yr}$. Therefore, this observationally motivated constraint affects also the progenitors of several other important populations, such as the double white dwarf binaries or cataclysmic variables.

Summary of the key results in the papers

Mass transfer in white dwarf-neutron star binaries.

(Bobrick et al., 2017) (Paper I)

1. WD-NS binaries with a WD more massive than $0.2 - 0.3 M_{\odot}$ result in unstable mass transfer leading to a tidal shredding of the WD.
2. The tension in the observed inspiral rates of binary millisecond pulsars with a WD companion and the UCXBs was resolved.
3. The Oil-on-Water code for modelling mass transfer was upgraded with the most recent numerical prescriptions, including original approaches introduced in the paper, e.g. a new method of initialising mass transfer in binaries.
4. Obtaining the main result required verifying Ritter's formula (Ritter, 1988) down to 5 – 10 per cent accuracy, obtaining a new model for orbit-averaged mass transfer rates in eccentric binaries and showing that stars may increase their volumetric radii by 10 – 15 per cent when tidally deformed by a companion.

Observed binary populations reflect the Galactic history. Explaining the orbital period-mass ratio relation in wide hot subdwarf binaries.

(Vos et al., 2020) (Paper II)

1. Period-mass ratio relation and period-metallicity relation in long-period sdB-MS binaries explained quantitatively for the first time.
2. sdB-MS binaries shown to reflect the metallicity history of the Galaxy.
3. Galactic metallicity history shown to have about 20 per cent effect on the periods of all binaries produced by stable RG mass transfer.
4. Binaries with an MS accretor of up to $1.5 M_{\odot}$ are shown to be strongly non-conservative at mass transfer rates $\gtrsim 10^{-5} M_{\odot}/\text{yr}$.
5. The observed long-period sdB stars connected to their progenitor properties.

Transients from ONe White-Dwarf - Neutron-Star/Black-Hole Mergers (Bohrick et al., 2021b) (Paper III)

1. Transient events from ONe WD-NS mergers must have already been detected. Alternatively, non-detection would put significant constraints on the merger process.
2. The faint end of type Ia supernovae is the most likely counterpart of ONe WD-NS mergers.
3. First hydrodynamic simulations of ONe WD-NS mergers, the resulting nuclear yields and synthetic multi-band light curves and spectra from such mergers.
4. SN AT2019kzr, a candidate event for a WD-NS/BH merger, can only be produced by WD-BH binaries and only assuming additional non-nuclear energy source in the first days after the merger.
5. Mergers of ONe WD-NS binaries may significantly contribute to the enrichment of the Galaxy by ^{53}Mn and, potentially, some other elements.

Production of Rapidly-Spinning Runaway Red Supergiants (Bohrick et al., 2021a) (Paper IV)

1. Betelgeuse is consistent with being produced in the ONC-1 cluster, initially as a high mass ratio binary.
2. Massive stars are ejected from their birth clusters at $v > 30$ km/s by dynamical encounters, thus becoming runaway stars. It is expected that of order a few per cent of runaway red supergiants may be rapidly spinning like Betelgeuse.
3. Isolated RSGs are more rarely rapidly-spinning compared to runaway RSGs.
4. The observed numbers of runaway Be stars and the observed number of peculiar giants are consistent with them being produced through dynamical interactions in clusters.

References

- Abate, C., Pols, O. R., Izzard, R. G., Mohamed, S. S., & de Mink, S. E. 2013, *A&A*, 552, A26, doi: 10.1051/0004-6361/201220007
- Agrawal, P., Hurley, J., Stevenson, S., Szécsi, D., & Flynn, C. 2020, *MNRAS*, 497, 4549, doi: 10.1093/mnras/staa2264
- Arnett, W. D. 1982, *ApJ*, 253, 785, doi: 10.1086/159681
- Askar, A., Szkudlarek, M., Gondek-Rosińska, D., Giersz, M., & Bulik, T. 2017, *MNRAS*, 464, L36, doi: 10.1093/mnras/slw177
- Asplund, M., Grevesse, N., Sauval, A. J., & Scott, P. 2009, *ARA&A*, 47, 481, doi: 10.1146/annurev.astro.46.060407.145222
- Bailer-Jones, C. A. L., Rybizki, J., Foesneau, M., Demleitner, M., & Andrae, R. 2021, *AJ*, 161, 147, doi: 10.3847/1538-3881/abd806
- Banerjee, S. 2018, *MNRAS*, 473, 909, doi: 10.1093/mnras/stx2347
- Bavera, S. S., Fragos, T., Zevin, M., et al. 2021, *A&A*, 647, A153, doi: 10.1051/0004-6361/202039804
- Bellm, E. C., Kulkarni, S. R., Graham, M. J., et al. 2019, *PASP*, 131, 018002, doi: 10.1088/1538-3873/aaecbe
- Bensby, T., Feltzing, S., & Lundström, I. 2003, *A&A*, 410, 527, doi: 10.1051/0004-6361:20031213
- Benz, W., Bowers, R. L., Cameron, A. G. W., & Press, W. H. . 1990, *ApJ*, 348, 647, doi: 10.1086/168273
- Blaauw, A. 1961, *BAN*, 15, 265
- Blinnikov, S. I., & Bartunov, O. S. 1993, *A&A*, 273, 106
- Bobrick, A., Davies, M. B., & Church, R. P. 2017, *MNRAS*, 467, 3556, doi: 10.1093/mnras/stx312

- Bobrick, A., Raddi, R., Chatzopoulos, E., et al. 2021a, To be Submitted
- Bobrick, A., Zenati, Y., Perets, H. B., Davies, M. B., & Church, R. 2021b, arXiv e-prints, arXiv:2104.03415. <https://arxiv.org/abs/2104.03415>
- Boubert, D., & Evans, N. W. 2018, MNRAS, 477, 5261, doi: 10.1093/mnras/sty980
- Broekgaarden, F. S., Justham, S., de Mink, S. E., et al. 2019, MNRAS, 490, 5228, doi: 10.1093/mnras/stz2558
- Cabezón, R. M., García-Senz, D., & Figueira, J. 2017, A&A, 606, A78, doi: 10.1051/0004-6361/201630208
- Cameron, A. G. W., & Mock, M. 1967, Nature, 215, 464, doi: 10.1038/215464a0
- Casares, J., Jonker, P. G., & Israelian, G. 2017, X-Ray Binaries, ed. A. W. Alsabti & P. Murdin, 1499, doi: 10.1007/978-3-319-21846-5_111
- Chambers, K. C., Magnier, E. A., Metcalfe, N., et al. 2016, arXiv e-prints, arXiv:1612.05560. <https://arxiv.org/abs/1612.05560>
- Chatzopoulos, E., Frank, J., Marcello, D. C., & Clayton, G. C. 2020, arXiv e-prints, arXiv:2005.04172. <https://arxiv.org/abs/2005.04172>
- Chen, X., Han, Z., Deca, J., & Podsiadlowski, P. 2013, MNRAS, 434, 186, doi: 10.1093/mnras/stt992
- Cherepashchuk, A., Postnov, K., Molkov, S., Antokhina, E., & Belinski, A. 2020, NewAR, 89, 101542, doi: 10.1016/j.newar.2020.101542
- Chevalier, R. A. 1982, ApJ, 258, 790, doi: 10.1086/160126
- Chini, R., Hoffmeister, V. H., Nasser, A., Stahl, O., & Zinnecker, H. 2012, MNRAS, 424, 1925, doi: 10.1111/j.1365-2966.2012.21317.x
- Choi, J., Dotter, A., Conroy, C., et al. 2016, ApJ, 823, 102, doi: 10.3847/0004-637X/823/2/102
- Chruslinska, M., Nelemans, G., & Belczynski, K. 2019, MNRAS, 482, 5012, doi: 10.1093/mnras/sty3087
- Church, R. P., Dischler, J., Davies, M. B., et al. 2009, MNRAS, 395, 1127, doi: 10.1111/j.1365-2966.2009.14619.x
- Comerón, F., & Figueras, F. 2020, A&A, 638, A90, doi: 10.1051/0004-6361/202038136
- Costa, G., Bressan, A., Mapelli, M., et al. 2021, MNRAS, 501, 4514, doi: 10.1093/mnras/staa3916
- Cullen, L., & Dehnen, W. 2010, MNRAS, 408, 669, doi: 10.1111/j.1365-2966.2010.17158.x
- Dan, M., Rosswog, S., Brügggen, M., & Podsiadlowski, P. 2014, MNRAS, 438, 14, doi: 10.1093/mnras/stt1766

- Dan, M., Rosswog, S., Guillochon, J., & Ramirez-Ruiz, E. 2011, *ApJ*, 737, 89, doi: 10.1088/0004-637X/737/2/89
- Davies, M. B. 1995, *MNRAS*, 276, 887, doi: 10.1093/mnras/276.3.887
- . 2013, *Globular Cluster Dynamical Evolution*, ed. T. D. Oswalt & G. Gilmore, Vol. 5, 879, doi: 10.1007/978-94-007-5612-0_17
- Davis, P. J., Siess, L., & Deschamps, R. 2013, *A&A*, 556, A4, doi: 10.1051/0004-6361/201220391
- De, K., Kasliwal, M. M., Tzanidakis, A., et al. 2020, arXiv e-prints, arXiv:2004.09029. <https://arxiv.org/abs/2004.09029>
- Decin, L., Cox, N. L. J., Royer, P., et al. 2012, *A&A*, 548, A113, doi: 10.1051/0004-6361/201219792
- Dehnen, W., & Aly, H. 2012, *MNRAS*, 425, 1068, doi: 10.1111/j.1365-2966.2012.21439.x
- Deschamps, R., Siess, L., Davis, P. J., & Jorissen, A. 2013, *A&A*, 557, A40, doi: 10.1051/0004-6361/201321509
- Dexter, J., & Kasen, D. 2013, *ApJ*, 772, 30, doi: 10.1088/0004-637X/772/1/30
- Dosopoulou, F., & Kalogera, V. 2016, *ApJ*, 825, 71, doi: 10.3847/0004-637X/825/1/71
- Edvardsson, B., Andersen, J., Gustafsson, B., et al. 1993, *A&A*, 500, 391
- Eggleton, P. P. 1971, *MNRAS*, 151, 351, doi: 10.1093/mnras/151.3.351
- . 1972, *MNRAS*, 156, 361, doi: 10.1093/mnras/156.3.361
- . 1983, *ApJ*, 268, 368, doi: 10.1086/160960
- El Mellah, I., Sundqvist, J. O., & Keppens, R. 2019, *A&A*, 622, L3, doi: 10.1051/0004-6361/201834543
- Eldridge, J. J., Stanway, E. R., Xiao, L., et al. 2017, *PASA*, 34, e058, doi: 10.1017/pasa.2017.51
- Faulkner, J. 1971, *ApJL*, 170, L99, doi: 10.1086/180848
- Fregeau, J. M., Joshi, K. J., Portegies Zwart, S. F., & Rasio, F. A. 2002, *ApJ*, 570, 171, doi: 10.1086/339576
- Fregeau, J. M., & Rasio, F. A. 2007, *ApJ*, 658, 1047, doi: 10.1086/511809
- Frohmaier, C., Sullivan, M., Maguire, K., & Nugent, P. 2018, *ApJ*, 858, 50, doi: 10.3847/1538-4357/aabc0b
- Fryxell, B., Olson, K., Ricker, P., et al. 2000, *ApJS*, 131, 273, doi: 10.1086/317361
- Fu, X., Bressan, A., Marigo, P., et al. 2018, *MNRAS*, 476, 496, doi: 10.1093/mnras/sty235

- Fujimoto, M. Y., Iben, I., J., & Becker, S. A. 1981, Response of low-mass main sequence stars to accretion, ed. C. Chiosi & R. Stalio, Vol. 89, 401–403, doi: 10.1007/978-94-009-8500-1_58
- Fuller, J., & Lai, D. 2012, MNRAS, 421, 426, doi: 10.1111/j.1365-2966.2011.20320.x
- . 2013, MNRAS, 430, 274, doi: 10.1093/mnras/sts606
- Gaia Collaboration. 2016, A&A, 595, A1, doi: 10.1051/0004-6361/201629272
- Geier, S., Østensen, R. H., Nemeth, P., et al. 2017, A&A, 600, A50, doi: 10.1051/0004-6361/201630135
- Giersz, M. 2001, MNRAS, 324, 218, doi: 10.1046/j.1365-8711.2001.04337.x
- Ginat, Y. B., & Perets, H. B. 2020, arXiv e-prints, arXiv:2011.00010. <https://arxiv.org/abs/2011.00010>
- Gingold, R. A., & Monaghan, J. J. 1977, MNRAS, 181, 375, doi: 10.1093/mnras/181.3.375
- Gvaramadze, V. V., Weidner, C., Kroupa, P., & Pflamm-Altenburg, J. 2012, MNRAS, 424, 3037, doi: 10.1111/j.1365-2966.2012.21452.x
- Hamers, A. S., & Dosopoulou, F. 2019, ApJ, 872, 119, doi: 10.3847/1538-4357/ab001d
- Hamers, A. S., Rantala, A., Neunteufel, P., Preece, H., & Vynatheya, P. 2021, MNRAS, 502, 4479, doi: 10.1093/mnras/stab287
- Han, Z., Podsiadlowski, P., Maxted, P. F. L., & Marsh, T. R. 2003, MNRAS, 341, 669, doi: 10.1046/j.1365-8711.2003.06451.x
- Han, Z., Podsiadlowski, P., Maxted, P. F. L., Marsh, T. R., & Ivanova, N. 2002, MNRAS, 336, 449, doi: 10.1046/j.1365-8711.2002.05752.x
- Harper, G. M., Brown, A., Guinan, E. F., et al. 2017, AJ, 154, 11, doi: 10.3847/1538-3881/aa6ff9
- Heber, U. 2009, ARA&A, 47, 211, doi: 10.1146/annurev-astro-082708-101836
- Heinke, C. O., Ivanova, N., Engel, M. C., et al. 2013, ApJ, 768, 184, doi: 10.1088/0004-637X/768/2/184
- Hillier, D. J., & Lanz, T. 2001, in Astronomical Society of the Pacific Conference Series, Vol. 247, Spectroscopic Challenges of Photoionized Plasmas, ed. G. Ferland & D. W. Savin, 343
- Hobbs, G., Lorimer, D. R., Lyne, A. G., & Kramer, M. 2005, MNRAS, 360, 974, doi: 10.1111/j.1365-2966.2005.09087.x
- Hopkins, P. F. 2013, MNRAS, 428, 2840, doi: 10.1093/mnras/sts210
- . 2015, MNRAS, 450, 53, doi: 10.1093/mnras/stv195

- Hurley, J. R., Pols, O. R., & Tout, C. A. 2000, *MNRAS*, 315, 543, doi: 10.1046/j.1365-8711.2000.03426.x
- Hurley, J. R., Tout, C. A., & Pols, O. R. 2002, *MNRAS*, 329, 897, doi: 10.1046/j.1365-8711.2002.05038.x
- Hut, P. 1981, *A&A*, 99, 126
- Iaria, R., Sanna, A., Di Salvo, T., et al. 2021, *A&A*, 646, A120, doi: 10.1051/0004-6361/202039225
- Istrate, A. G., Marchant, P., Tauris, T. M., et al. 2016, *A&A*, 595, A35, doi: 10.1051/0004-6361/201628874
- Istrate, A. G., Tauris, T. M., Langer, N., & Antoniadis, J. 2014, *A&A*, 571, L3, doi: 10.1051/0004-6361/201424681
- Ivanova, N., Heinke, C. O., Rasio, F. A., Belczynski, K., & Fregeau, J. M. 2008, *MNRAS*, 386, 553, doi: 10.1111/j.1365-2966.2008.13064.x
- Ivanova, N., Heinke, C. O., Rasio, F. A., et al. 2006, *MNRAS*, 372, 1043, doi: 10.1111/j.1365-2966.2006.10876.x
- Ivanova, N., Justham, S., Chen, X., et al. 2013, *A&A Rv*, 21, 59, doi: 10.1007/s00159-013-0059-2
- Jones, D., & Boffin, H. M. J. 2017, *Nature Astronomy*, 1, 0117, doi: 10.1038/s41550-017-0117
- Joyce, M., Leung, S.-C., Molnár, L., et al. 2020, *ApJ*, 902, 63, doi: 10.3847/1538-4357/abb8db
- Kaaret, P., Feng, H., & Roberts, T. P. 2017, *ARA&A*, 55, 303, doi: 10.1146/annurev-astro-091916-055259
- Kalogera, V., Narayan, R., Spergel, D. N., & Taylor, J. H. 2001, *ApJ*, 556, 340, doi: 10.1086/321583
- Kasen, D., Thomas, R. C., & Nugent, P. 2006, *ApJ*, 651, 366, doi: 10.1086/506190
- Kenyon, S. J. 1986, *The symbiotic stars*
- Kervella, P., Decin, L., Richards, A. M. S., et al. 2018, *A&A*, 609, A67, doi: 10.1051/0004-6361/201731761
- Kim, C., Kalogera, V., Lorimer, D. R., & White, T. 2004, *ApJ*, 616, 1109, doi: 10.1086/424954
- Kippenhahn, R., & Meyer-Hofmeister, E. 1977, *A&A*, 54, 539
- Kippenhahn, R., Weigert, A., & Weiss, A. 2012, *Stellar Structure and Evolution*, doi: 10.1007/978-3-642-30304-3
- Klencki, J., Nelemans, G., Istrate, A. G., & Chruslinska, M. 2021, *A&A*, 645, A54, doi: 10.1051/0004-6361/202038707

- Kolb, U., & Ritter, H. 1990, *A&A*, 236, 385
- Kopal, Z. 1959, *Close binary systems*
- Kroupa, P. 2001, *MNRAS*, 322, 231, doi: 10.1046/j.1365-8711.2001.04022.x
- Kuranov, A. K., Postnov, K. A., & Yungelson, L. R. 2020, arXiv e-prints, arXiv:2010.03488.
<https://arxiv.org/abs/2010.03488>
- Lajoie, C.-P., & Sills, A. 2011, *ApJ*, 726, 67, doi: 10.1088/0004-637X/726/2/67
- Lallement, R., Vergely, J. L., Valette, B., et al. 2014, *A&A*, 561, A91, doi: 10.1051/0004-6361/201322032
- Lambert, D. L., Brown, J. A., Hinkle, K. H., & Johnson, H. R. 1984, *ApJ*, 284, 223, doi: 10.1086/162401
- Landau, L. D., & Lifshitz, E. M. 1987, *Fluid Mechanics*
- Laplace, E., Götberg, Y., de Mink, S. E., Justham, S., & Farmer, R. 2020, *A&A*, 637, A6, doi: 10.1051/0004-6361/201937300
- Law, N. M., Kulkarni, S. R., Dekany, R. G., et al. 2009, *PASP*, 121, 1395, doi: 10.1086/648598
- Leonard, P. J. T., & Duncan, M. J. 1990, *AJ*, 99, 608, doi: 10.1086/115354
- LSST Science Collaboration. 2009, arXiv e-prints, arXiv:0912.0201.
<https://arxiv.org/abs/0912.0201>
- Lubow, S. H., & Shu, F. H. 1975, *ApJ*, 198, 383, doi: 10.1086/153614
- Lucy, L. B. 1977, *AJ*, 82, 1013, doi: 10.1086/112164
- Maoz, D., Mannucci, F., & Brandt, T. D. 2012, *MNRAS*, 426, 3282, doi: 10.1111/j.1365-2966.2012.21871.x
- Metzger, B. D. 2012, *MNRAS*, 419, 827, doi: 10.1111/j.1365-2966.2011.19747.x
- Milislavljevic, D., & Margutti, R. 2018, *SSRv*, 214, 68, doi: 10.1007/s11214-018-0500-y
- Moe, M., & Di Stefano, R. 2017, *ApJS*, 230, 15, doi: 10.3847/1538-4365/aa6fb6
- Moe, M., Kratter, K. M., & Badenes, C. 2019, *ApJ*, 875, 61, doi: 10.3847/1538-4357/ab0d88
- Mohamed, S., Mackey, J., & Langer, N. 2012, *A&A*, 541, A1, doi: 10.1051/0004-6361/201118002
- Monaghan, J. J. 1992, *ARA&A*, 30, 543, doi: 10.1146/annurev.aa.30.090192.002551
- Moriya, T., Tominaga, N., Blinnikov, S. I., Baklanov, P. V., & Sorokina, E. I. 2011, *MNRAS*, 415, 199, doi: 10.1111/j.1365-2966.2011.18689.x

- Munari, U. 2019, arXiv e-prints, arXiv:1909.01389. <https://arxiv.org/abs/1909.01389>
- Nelson, L. A., Rappaport, S. A., & Joss, P. C. 1986, *ApJ*, 304, 231, doi: 10.1086/164156
- Nomoto, K., Kobayashi, C., & Tominaga, N. 2013, *ARA&A*, 51, 457, doi: 10.1146/annurev-astro-082812-140956
- Nomoto, K., Thielemann, F. K., & Yokoi, K. 1984, *ApJ*, 286, 644, doi: 10.1086/162639
- Oh, S., & Kroupa, P. 2016, *A&A*, 590, A107, doi: 10.1051/0004-6361/201628233
- Paczynski, B. 1991, *ApJ*, 370, 597, doi: 10.1086/169846
- Pavlovskii, K., Ivanova, N., Belczynski, K., & Van, K. X. 2017, *MNRAS*, 465, 2092, doi: 10.1093/mnras/stw2786
- Paxton, B., Bildsten, L., Dotter, A., et al. 2011, *ApJS*, 192, 3, doi: 10.1088/0067-0049/192/1/3
- Paxton, B., Cantiello, M., Arras, P., et al. 2013, *ApJS*, 208, 4, doi: 10.1088/0067-0049/208/1/4
- Paxton, B., Marchant, P., Schwab, J., et al. 2015, *ApJS*, 220, 15, doi: 10.1088/0067-0049/220/1/15
- Paxton, B., Schwab, J., Bauer, E. B., et al. 2018, *ApJS*, 234, 34, doi: 10.3847/1538-4365/aaa5a8
- Paxton, B., Smolec, R., Schwab, J., et al. 2019, *ApJS*, 243, 10, doi: 10.3847/1538-4365/ab2241
- Pejcha, O., Metzger, B. D., Tyles, J. G., & Tomida, K. 2017, *ApJ*, 850, 59, doi: 10.3847/1538-4357/aa95b9
- Peters, P. C. 1964, *Physical Review*, 136, 1224, doi: 10.1103/PhysRev.136.B1224
- Podsiadlowski, P., Rappaport, S., & Pfahl, E. D. 2002, *ApJ*, 565, 1107, doi: 10.1086/324686
- Pols, O. R., & Marinus, M. 1994, *A&A*, 288, 475
- Popham, R., & Narayan, R. 1991, *ApJ*, 370, 604, doi: 10.1086/169847
- Poveda, A., Ruiz, J., & Allen, C. 1967, *Boletín de los Observatorios Tonantzintla y Tacubaya*, 4, 86
- Price, D. J. 2012, *Journal of Computational Physics*, 231, 759, doi: 10.1016/j.jcp.2010.12.011
- Raghavan, D., McAlister, H. A., Henry, T. J., et al. 2010, *ApJS*, 190, 1, doi: 10.1088/0067-0049/190/1/1
- Rappaport, S., Joss, P. C., & Webbink, R. F. 1982, *ApJ*, 254, 616, doi: 10.1086/159772
- Rappaport, S., Podsiadlowski, P., Joss, P. C., Di Stefano, R., & Han, Z. 1995, *MNRAS*, 273, 731, doi: 10.1093/mnras/273.3.731
- Rappaport, S., Verbunt, F., & Joss, P. C. 1983, *ApJ*, 275, 713, doi: 10.1086/161569

- Rau, A., Kulkarni, S. R., Law, N. M., et al. 2009, *PASP*, 121, 1334, doi: 10.1086/605911
- Regös, E., Bailey, V. C., & Mardling, R. 2005, *MNRAS*, 358, 544, doi: 10.1111/j.1365-2966.2005.08813.x
- Renzo, M., Zapartas, E., de Mink, S. E., et al. 2019, *A&A*, 624, A66, doi: 10.1051/0004-6361/201833297
- Repetto, S., Davies, M. B., & Sigurdsson, S. 2012, *MNRAS*, 425, 2799, doi: 10.1111/j.1365-2966.2012.21549.x
- Ritter, H. 1988, *A&A*, 202, 93
- Rivinius, T., Carciofi, A. C., & Martayan, C. 2013, *A&A Rv*, 21, 69, doi: 10.1007/s00159-013-0069-0
- Robin, A. C., Reylé, C., Derrière, S., & Picaud, S. 2003, *A&A*, 409, 523, doi: 10.1051/0004-6361:20031117
- Rosswog, S. 2020, *MNRAS*, 498, 4230, doi: 10.1093/mnras/staa2591
- Rosswog, S., & Diener, P. 2020, arXiv e-prints, arXiv:2012.13954. <https://arxiv.org/abs/2012.13954>
- Rosswog, S., Liebendörfer, M., Thielemann, F. K., et al. 1999, *A&A*, 341, 499. <https://arxiv.org/abs/astro-ph/9811367>
- Saitoh, T. R., & Makino, J. 2009, *ApJL*, 697, L99, doi: 10.1088/0004-637X/697/2/L99
- Sana, H., de Mink, S. E., de Koter, A., et al. 2012, *Science*, 337, 444, doi: 10.1126/science.1223344
- Savonije, G. J., de Kool, M., & van den Heuvel, E. P. J. 1986, *A&A*, 155, 51
- Seitenzahl, I. R., Cescutti, G., Röpke, F. K., Ruiter, A. J., & Pakmor, R. 2013a, *A&A*, 559, L5, doi: 10.1051/0004-6361/201322599
- Seitenzahl, I. R., Ciaraldi-Schoolmann, F., Röpke, F. K., et al. 2013b, *MNRAS*, 429, 1156, doi: 10.1093/mnras/sts402
- Sengar, R., Tauris, T. M., Langer, N., & Istrate, A. G. 2017, *MNRAS*, 470, L6, doi: 10.1093/mnrasl/slx064
- Sepinsky, J. F., Willems, B., & Kalogera, V. 2007a, *ApJ*, 660, 1624, doi: 10.1086/513736
- Sepinsky, J. F., Willems, B., Kalogera, V., & Rasio, F. A. 2007b, *ApJ*, 667, 1170, doi: 10.1086/520911
- Shakura, N. I., & Sunyaev, R. A. 1973, *A&A*, 500, 33
- Shibata, M., & Hotokezaka, K. 2019, *Annual Review of Nuclear and Particle Science*, 69, 41, doi: 10.1146/annurev-nucl-101918-023625

- Shiber, S., & Soker, N. 2018, *MNRAS*, 477, 2584, doi: 10.1093/mnras/sty843
- Smith, K. W., Smartt, S. J., Young, D. R., et al. 2020, *PASP*, 132, 085002, doi: 10.1088/1538-3873/ab936e
- Soberman, G. E., Phinney, E. S., & van den Heuvel, E. P. J. 1997, *A&A*, 327, 620. <https://arxiv.org/abs/astro-ph/9703016>
- Springel, V. 2005, *MNRAS*, 364, 1105, doi: 10.1111/j.1365-2966.2005.09655.x
- . 2010, *MNRAS*, 401, 791, doi: 10.1111/j.1365-2966.2009.15715.x
- Springel, V., & Hernquist, L. 2002, *MNRAS*, 333, 649, doi: 10.1046/j.1365-8711.2002.05445.x
- Stone, N. C., & Leigh, N. W. C. 2019, *Nature*, 576, 406, doi: 10.1038/s41586-019-1833-8
- Tauris, T. M., & van den Heuvel, E. P. J. 2006, *Formation and evolution of compact stellar X-ray sources*, Vol. 39, 623–665
- Timmes, F. X. 1999, *ApJS*, 124, 241, doi: 10.1086/313257
- Timmes, F. X., Hoffman, R. D., & Woosley, S. E. 2000, *ApJS*, 129, 377, doi: 10.1086/313407
- Timmes, F. X., & Swesty, F. D. 2000, *ApJS*, 126, 501, doi: 10.1086/313304
- Toonen, S., Hamers, A., & Portegies Zwart, S. 2016, *Computational Astrophysics and Cosmology*, 3, 6, doi: 10.1186/s40668-016-0019-0
- Toonen, S., Nelemans, G., & Portegies Zwart, S. 2012, *A&A*, 546, A70, doi: 10.1051/0004-6361/201218966
- Toonen, S., Perets, H. B., Igoshev, A. P., Michaely, E., & Zenati, Y. 2018, *A&A*, 619, A53, doi: 10.1051/0004-6361/201833164
- Toonen, S., Portegies Zwart, S., Hamers, A. S., & Bandopadhyay, D. 2020, *A&A*, 640, A16, doi: 10.1051/0004-6361/201936835
- Uitenbroek, H., Dupree, A. K., & Gilliland, R. L. 1998, *AJ*, 116, 2501, doi: 10.1086/300596
- Van, K. X., Ivanova, N., & Heinke, C. O. 2019, *MNRAS*, 483, 5595, doi: 10.1093/mnras/sty3489
- van den Heuvel, E. P. J. 1994, in *Saas-Fee Advanced Course 22: Interacting Binaries*, 263–474
- van Haften, L. M., Nelemans, G., Voss, R., et al. 2013, *A&A*, 552, A69, doi: 10.1051/0004-6361/201220552
- van Haften, L. M., Nelemans, G., Voss, R., Wood, M. A., & Kuijpers, J. 2012, *A&A*, 537, A104, doi: 10.1051/0004-6361/201117880
- Vink, J. S., de Koter, A., & Lamers, H. J. G. L. M. 2001, *A&A*, 369, 574, doi: 10.1051/0004-6361:20010127

- Vos, J., Bobrick, A., & Vučković, M. 2020, *A&A*, 641, A163, doi: 10.1051/0004-6361/201937195
- Vos, J., Németh, P., Vučković, M., Østensen, R., & Parsons, S. 2018, *MNRAS*, 473, 693, doi: 10.1093/mnras/stx2198
- Vos, J., Østensen, R. H., Marchant, P., & Van Winckel, H. 2015, *A&A*, 579, A49, doi: 10.1051/0004-6361/201526019
- Vos, J., Østensen, R. H., Vučković, M., & Van Winckel, H. 2017, *A&A*, 605, A109, doi: 10.1051/0004-6361/201730958
- Wang, L., Spurzem, R., Aarseth, S., et al. 2016, *MNRAS*, 458, 1450, doi: 10.1093/mnras/stw274
- Webbink, R. F. 1985, *Stellar evolution and binaries*, ed. J. E. Pringle & R. A. Wade, 39
- Wenger, M., Ochsenbein, F., Egret, D., et al. 2000, *A&AS*, 143, 9, doi: 10.1051/aas:2000332
- Wollaeger, R. T., & van Rossum, D. R. 2014, *ApJS*, 214, 28, doi: 10.1088/0067-0049/214/2/28
- Wollaeger, R. T., van Rossum, D. R., Graziani, C., et al. 2013, *ApJS*, 209, 36, doi: 10.1088/0067-0049/209/2/36
- Zahn, J. P. 1975, *A&A*, 41, 329
- Zenati, Y., Bobrick, A., & Perets, H. B. 2020, *MNRAS*, 493, 3956, doi: 10.1093/mnras/staa507
- Zenati, Y., Perets, H. B., & Toonen, S. 2019, *MNRAS*, 486, 1805, doi: 10.1093/mnras/stz316

Scientific publications

Paper summaries and author contributions

Paper 1:

Mass transfer in white dwarf-neutron star binaries

Alexey Bobrick, Melvyn B. Davies, and Ross Church (2017)
MNRAS, 467(3), p. 3556–3575.

Starting from an older version of the smoothed particle hydrodynamics (SPH) code Oil-on-Water, Alexey Bobrick converted it to a modern form. He adopted the most recent prescriptions in the literature. Specifically, he converted the code to a Lagrangian-based formulation, the integrator, equation of state, shock treatment, Oil-on-Water treatment were rewritten, the gravity tree was split, the code was profiled and optimised for performance, and a new rendering tool was constructed. The simulations were carried out in coordination with Melvyn B. Davies. Alexey Bobrick developed the formalism for the effects of eccentricity, a new method for setting up and relaxing single and binary stars, and the first version of the secular evolution model; the production version of the secular code was implemented by Ross Church in coordination with Alexey Bobrick and Melvyn B. Davies. The paper structure, the paper text and the comparison to observations were performed in close coordination with the co-authors, with Ross Church writing sections 6.1-6.4.

Paper 2:

Observed binary populations reflect the Galactic history. Explaining the orbital period-mass ratio relation in wide hot subdwarf binaries

Joris Vos, Alexey Bobrick, and Maja Vuckovic (2020)

Joris Vos had earlier developed a method for modelling red giant mass transfer onto main-sequence stars with MESA code, constructing photometric and spectral identifications of mass transfer products. Joris Vos and Maja Vuckovic had earlier built an observational dataset of long-period subdwarf B binaries. In the study, Alexey Bobrick proposed a new model for red giant mass transfer and provided constraints for mass transfer parameters in the study. In coordination with Alexey Bobrick and Maja Vuckovic, Joris Vos updated the MESA code to follow the new model of mass transfer and developed functionality to execute and process large grids of MESA runs. Alexey Bobrick proposed accounting for the Galactic chemical evolution to explain the observed properties of sdB binaries and provided a Galactic population of their progenitors for further simulations. Writing of the manuscript was done with equal contributions from three co-authors, with Alexey Bobrick developing parts of Section 1 (introduction), most of Section 3 (binary evolution model), Section 4 (galactic evolution model), parts of Section 5 and 6 (MESA simulations, results) and a large part of the discussion section 7.

Paper 3:

Transients from ONE White Dwarf-Neutron Star Mergers

Alexey Bobrick, Yossef Zenati, Hagai B. Perets, Melvyn B. Davies, Ross Church

Submitted to MNRAS.

Alexey Bobrick has carried out hydrodynamic simulations with the Lagrangian SPH code Water, while Yossef Zenati carried out simulations with the Eulerian FLASH code for a subset of models. Alexey Bobrick updated the nuclear post-processing method to work with the efficient Torch code and carried out the post-processing and supernova spectral synthesis simulations with SuperNu code. Alexey Bobrick, in close coordination with Yossef Zenati, compared the performance of the SPH and FLASH codes. Alexey Bobrick analysed the simulations and wrote most of the paper. All co-authors contributed equally to discussion section 4 (comparison to observations).

Paper 4:

Production of Rapidly-Spinning Runaway Red Supergiants

Alexey Bobrick, Roberto Raddi, Emmanouil Chatzopoulos, Ross Church,

Melvyn B. Davies, Juhan Frank

To be submitted to MNRAS.

Alexey Bobrick developed a population of stars and a Monte Carlo generator for dynamical encounters in Galactic clusters. He has applied the existing FewBody code to these encounters. Together with Manos Chatzopoulos, he developed an evolutionary model for massive binaries and their merger outcomes. Together with Roberto Raddi, he constructed the Galactic trajectories, the photometric appearance in the Galaxy, accounting for dust extinction. Roberto Raddi obtained the Gaia eDR3-based volume-limited sample of observed Galactic red supergiants. Alexey Bobrick and Roberto Raddi compared the synthetic and the observed samples. Alexey Bobrick wrote most of the paper.



Faculty of Science
Department of Astronomy
and Theoretical Physics

ISBN 978-91-7895-901-3

